Catalysis Science & Technology

PAPER

View Article Online
View Journal | View Issue

Published on 14 June 2016. Downloaded by Centro de Investigaciones Biologicas (CIB) on 14/09/2016 13:11:33.

Cite this: *Catal. Sci. Technol.*, 2016, **6**, 6625

Alkaline versatile peroxidase by directed evolution†

David Gonzalez-Perez,[a] Ivan Mateljak,[a] Eva Garcia-Ruiz,[b] Francisco J. Ruiz-Dueñas,[c] Angel T. Martinez[c] and Miguel Alcalde*[a]

Received 12th May 2016,
Accepted 10th June 2016

DOI: 10.1039/c6cy01044j

www.rsc.org/catalysis

Ligninolytic peroxidases are involved in natural wood decay in strict acid environments. Despite their biotechnological interest, these high-redox potential enzymes are not functional at basic pH due to the loss of calcium ions that affects their structural integrity. In this study, we have built catalytic activity at basic pH in a versatile peroxidase (VP) previously engineered for thermostability. By using laboratory evolution and hybrid approaches, we designed an active and highly stable alkaline VP while the catalytic bases behind the alkaline activation were unveiled. A stabilizing mutational backbone allowed the pentacoordinated heme state to be maintained, and the new alkaline mutations hyperactivated the enzyme after incubation at basic pHs. The final mutant oxidises substrates at alkaline pHs both at the heme channel and at the Mn^{2+} site, while the catalytic tryptophan was not operational under these conditions. Mutations identified in this work could be transferred to other ligninolytic peroxidases for alkaline activation.

1. Introduction

The ligninolytic secretome from basidiomycete white-rot fungi is responsible for carbon recycling in land ecosystems.[1,2] Mostly formed by high-redox potential oxidoreductases (peroxidases and laccases), along with enzymes supplying H_2O_2 and diffusible redox active species, this consortium decomposes lignin through a complex cascade of reactions that are carried out in a strict acid environment (pH ~3 due to the release of organic acids from fungal metabolism).[3,4] Within this efficient oxidative system, high-redox potential peroxidases play a fundamental role. Indeed, it has been recently reported that the primitive ancestry of these enzymes links them to the end of coal deposits on earth during the later Carboniferous era.[5,6] Currently, they are classified in class II (secreted fungal peroxidases) of the peroxidase–catalase superfamily that is made up of manganese peroxidases (MnPs, EC 1.11.1.13), lignin peroxidases (LiPs, EC 1.11.1.14) and versatile peroxidases (VPs, EC 1.11.1.16).[7,8] Of these, the latter are considered by far the most promiscuous peroxidases found in nature due to their high redox potential (+1.4 V) and broad substrate range.[9]

The one-electron oxidation reactions carried out by VP involve three different oxidation sites and several catalytic intermediates for the transformation of low-, medium- and high-redox potential compounds.[10] Within a compact and rather small protein structure that is enriched in α-helices (~300 residues tightly packed through four disulphide bridges and two embedded structural calcium cations) VP contains a heme group with a main access channel – 9 Å in diameter – that is involved in the oxidation of low-redox potential compounds; a Mn^{2+} binding site governed by three carboxylic residues for the oxidation of Mn^{2+} to Mn^{3+}; and a catalytic Trp at the protein surface, whose activated radical permits the oxidation of both low- and high-redox potential compounds at acid pH through a long-range electron transfer (LRET) pathway to the heme.[11–13] Thus, VP not only shares catalytic attributes with MnPs for the oxidation of Mn^{2+}, but it is also capable of oxidizing the redox mediator veratryl alcohol at the catalytic Trp (like LiPs) as well as several low-redox potential compounds at the heme access channel, like generic (low-redox potential) peroxidases (GPs, EC 1.11.1.7). In addition, and unlike LiPs, VP efficiently oxidizes several high-redox potential compounds at the catalytic Trp in the absence of veratryl alcohol, and also low-redox potential substrates with high efficiency. Recently, VP was shown to oxidize several lignosulfonates in the absence of mediators, which emphasizes its pivotal role within the ligninolytic consortium.[14] Taken together, these features make VP a quite interesting model for protein designers.

One of the most attractive and intriguing challenges in VP engineering, and indeed, that of all ligninolytic peroxidases

[a] *Department of Biocatalysis, Institute of Catalysis, CSIC, 28049 Madrid, Spain. E-mail: malcalde@icp.csic.es; Fax: +34 915854760; Tel: +34 915854806*
[b] *Department of Chemical and Biomolecular Engineering, University of Illinois at Urbana-Champaign, Urbana, IL 61801, USA*
[c] *Center for Biological Investigations, CSIC, Ramiro de Maeztu 9, 28040 Madrid, Spain*

† Electronic supplementary information (ESI) available. See DOI: 10.1039/c6cy01044j

Published on 14 June 2016. Downloaded by Centro de Investigaciones Biologicas (CIB) on 14/09/2016 13:11:33.

reported to date, is to achieve activity and stability at alkaline pHs. These features would open VP up to several biomedical purposes from the synthesis of injectable hydrogels for tissue engineering and drug delivery to enhance the chemiluminiscence signal in luminol-dependent reactions for forensic, pharmaceutical and analytical applications.[2,15–18] It is well known that the integrity of VP strongly depends on the correct attachment of the two structural Ca^{2+} located above and below the plane of the heme (in the distal and proximal domains, respectively).[19,20] The distal Ca^{2+} is fairly accessible to the solvent and it is coordinated by 7 oxygen atoms, involving two water molecules and four amino acids. By contrast, the proximal Ca^{2+} is located deep in the protein structure and it is coordinated by 8 oxygen atoms from five surrounding residues. Any subtle modification in the coordination spheres of these two cations affects the heme morphology and compromises the enzyme's functionality. Several studies have shown that both neutral/basic pH and high temperature favour Ca^{2+} loss, mostly that of the distal Ca^{2+}, leading to the hexacoordination of the heme in a low spin state (bis-histidyl heme iron complex). In this situation the heme cavity collapses, inactivating the enzyme (a phenomenon also observed in LiPs and MnPs).[21–23]

We previously performed *in vitro* evolution on the VP from the edible mushroom *Pleurotus eryngii* to improve its functional expression and thermostability in *Saccharomyces cerevisiae*.[24] After 6 generations, we obtained a VP mutant (named 2-1B) that was readily secreted by yeast and that had an 8 °C improvement in its thermostability. Notably, the 2-1B mutant was also remarkably stable, yet not active, at basic pHs. Very recently, we demonstrated that the E37K-H39R-G330R mutations in the thermostabilizing backbone were responsible for this alkaline stability, establishing new contacts while abrogating destabilizing interactions, thereby reinforcing the pentacoordinated heme state at basic pHs to avoid the calcium leakage.[25] Although the 2-1B variant retains its overall structural integrity at basic pHs; it is not active even at a neutral pH. Hence, using the stable 2-1B variant as our departure point, we have now designed the first ligninolytic peroxidase that is active at alkaline pH. We performed several rounds of directed evolution and rational mutagenesis and the final mutant obtained was characterized exhaustively to unveil the catalytic determinants underlying this unprecedented improvement.

2. Experimental

All chemical reagents were of the highest purity commercially available. Culture media were prepared as described in the ESI.†

2.1 Laboratory evolution and rational mutagenesis

All PCR fragments were cleaned, concentrated, and loaded onto a low melting point preparative agarose gel (0.75% w/v) and purified. Mutant libraries were cloned under the control of GAL1 promoter of the pJRoC30 expression shuttle vector replacing the parent gene. The pJRoC30 plasmid was linearized with *Bam*HI and *Xho*I, and the linear plasmid was concentrated and purified as described above for the PCR fragments. The parental type 2-1B mutant was previously obtained as described elsewhere.[24]

2.1.1 Mutagenic PCR (1st and 2nd generations). Reaction mixtures were prepared in a final volume of 50 μL containing DNA template (0.1 ng μL^{-1}), 90 nM forward RMLN primer (5′-CCTCTATACTTTAACGTCAAGG-3′), 90 nM reverse RMLC primer (5′-GGGAGGGCGTGAATGTAAGC-3′), 0.3 mM dNTPs (0.075 mM each), 3% (v/v) dimethyl sulfoxide (DMSO), 1.5 mM $MgCl_2$, 0.01 mM $MnCl_2$ and 0.05 U μL^{-1} *Taq* polymerase. The error-prone PCR reactions were carried out in a gradient thermocycler (Mycycler, BioRad, USA) under the following conditions: 95 °C for 2 min (1 cycle); 94 °C for 45 s, 50 °C for 45 s, 72 °C for 2 min (28 cycles); and 72 °C for 10 min (1 cycle). The PCR product was purified and cleaned and 200 ng of total DNA was used to transform *S. cerevisiae* together with 100 ng of linearized plasmid (ratio library : vector, 2 : 1) using the Yeast Transformation Kit (Sigma-Aldrich, Madrid, Spain). Transformed cells were plated on SC drop-out plates and incubated for 3 days at 30 °C. Subsequently, the mutant library was screened using the HTS-protocol for activity (see below).

2.1.2 *In vivo* assembly of mutant libraries (IvAM, 3rd generation). We followed the protocol described before with minor modifications.[26] i) Mutagenic PCR1. Reaction mixtures were prepared in a final volume of 50 μL containing DNA template (0.1 ng μL^{-1} 5B9-1G mutant), 90 nM RMLN primer, 90 nM RMLC primer, 0.3 mM dNTPs (0.075 mM each), 3% (v/v) dimethyl sulfoxide (DMSO), 1.5 mM $MgCl_2$, 0.01 mM $MnCl_2$ and 0.05 U μL^{-1} *Taq* polymerase. ii) Mutagenic PCR2. Reaction mixtures were prepared in a final volume of 50 μL containing DNA template (50.42 ng μL^{-1} 9B3-2G mutant), 0.37 μM RMLN primer, 0.37 μM RMLC primer, 0.8 mM dNTPs (0.2 mM each), 3% (v/v) dimethyl sulfoxide (DMSO), and 0.05 U μL^{-1} Mutazyme II. Error-prone PCRs were carried out using the following parameters: 95 °C for 2 min (1 cycle); 95 °C for 45 s, 50 °C for 30 s, 72 °C for 1 min 30 s (28 cycles); and 72 °C for 10 min (1 cycle). iii) *In vivo* recombination of mutant libraries in *S. cerevisiae*. Mutant libraries from PCR1 and PCR2 were added in equimolar concentrations (200 ng each) to the linearized vector (100 ng). Transformed cells were plated on SC drop-out plates and incubated for 3 days at 30 °C. Thereafter, the mutant libraries were subjected to the HTS-screening protocol (see below).

2.1.3 Saturation mutagenesis at position 182. Reaction mixtures were prepared in a final volume of 50 μL containing DNA template (2 ng μL^{-1} BB-8-3G mutant), 1 mM dNTPs (0.25 mM each), 3% (v/v) dimethyl sulfoxide (DMSO), and 0.05 U μL^{-1} *Pfu* Ultra DNA polymerase. The primers used were 0.25 μM RMLN, 0.25 μM SM182-VP R (5′-GTTGAATCGAATGGCATTCC **SNN** AATCGATGGGTCAACCTTGT-3′) reverse primer for PCR 1; and 0.25 μM SM182-VP F (5′-ACAAGGTTGACCCATCGATT **NNS** GGAATGCCATTCGATTCAAC-3′) forward primer, 0.25 μM RMLC for PCR2. Degenerate codons (N = A, T, G, C; S = G, C) are

 This journal is © The Royal Society of Chemistry 2016

Published on 14 June 2016. Downloaded by Centro de Investigaciones Biologicas (CIB) on 14/09/2016 13:11:33.

highlighted in bold and underlined. PCRs were performed on a gradient using the following conditions: 95 °C for 2 min (1 cycle); 94 °C for 45 s, 50 °C for 45 s, 72 °C for 1 min (28 cycles); and 72 °C for 10 min (1 cycle). The whole gene was *in vivo* reassembled by IVOE,[27] transforming *S. cerevisiae* cells independently with 200 ng of each PCR product and 100 ng of linearized pJRoC30 plasmid. Yeast cells were plated on SC drop-out plates and incubated for 3 days at 30 °C. Thereafter, the mutant libraries were subjected to the HTS-protocol as described below.

2.1.4 Site-directed mutagenesis (E36L-D175L-A173I). The mutant was produced by site-directed mutagenesis through IVOE.[27] Because of the distance between mutations, a double mutant was firstly designed (E36L-D175L) and used as a template for introducing the A173I mutation. The reaction mixture was prepared in a final volume of 50 μL containing DNA template (2 ng μL^{-1} BB-8-3G mutant), 1 mM dNTPs (0.25 mM each), 3% (v/v) dimethyl sulfoxide (DMSO), and 0.05 U μL^{-1} *Pfu* Ultra DNA polymerase. The primers used for site-directed mutagenesis of the double mutant were 0.25 μM RMLN, 0.25 μM E36L R reverse primer (5′-CGAAGGGACTCGCGCACCTT **TAG** TCCACACTGGGCACCGTCGA) for PCR1; 0.25 μM E36L F forward primer (5′-TCGACGGTGCCCAGTGTGGA **CTA** AAGGTGCGCGAGTCCCTTCG), 0.25 μM D175L R reverse primer (5′-GAAATCGATGGGTCAACCTT **GAG** GGCAGCGGCAATGGAGTGCG) for PCR2; and 0.25 μM D175L F forward primer (5′-CGCACTCCATTGCCGCTGCC **CTC** AAGGTTGACCCATCGATTTC), 0.25 μM RMLC for PCR3. Mutated codons are underlined and in bold. The three PCRs were performed with the following conditions: 95 °C for 2 min (1 cycle); 94 °C for 45 s, 50 °C for 45 s, 72 °C for 1 min (28 cycles); and 72 °C for 10 min (1 cycle). The whole gene was *in vivo* reassembled, transforming *S. cerevisiae* cells with 200 ng of each PCR product and 100 ng of linearized pJRoC30. Yeast cells were plated on SC drop-out plates and incubated for 3 days at 30 °C. Thereafter, the plasmid was recovered from the cells and used as template for the following PCR reactions: 0.25 μM RMLN forward primer (5′-CCTCTATACTTTAACGTCAAGG), 0.25 μM A173I R reverse primer (5′-GATGGGTCAACCTTGAGGGC **AAT** GGCAATGGAGTGCGAAGCCAG) for PCR 4; and 0.25 μM A173I F forward primer (5′-CTGGCTTCGCACTCCATTGCC **ATT** GCCCTCAAGGTTGACCCATC), 0.25 μM RMLC reverse primer (5′-GGGAGGGCGTGAATGTAAGC) for PCR 5. Mutated codons are in bold and underlined. The PCRs were performed with the following conditions: 95 °C for 2 min (1 cycle); 94 °C for 45 s, 50 °C for 45 s, 72 °C for 1 min (28 cycles); and 72 °C for 10 min (1 cycle). The whole gene was *in vivo* reassembled, transforming *S. cerevisiae* cells independently with 200 ng of PCR product 4 and 5 plus 100 ng of linearized pJRoC30 plasmid for each construction. Transformed cells were plated on SC drop-out plates and incubated for 3 days at 30 °C. Thereafter, the mutant libraries were subjected to the HTS-protocol as described below.

2.2 High-throughput screening protocol (HTS-protocol)

Individual clones were selected and cultured in sterile 96-well plates (Greiner Bio-One GmbH, Germany) containing 50 μL per well of SC minimal medium (SC-Hemin for the 1st generation). In each plate, column number 6 was inoculated with the parental 2-1B mutant as an internal standard, and well-H1 (containing minimal medium SC (or SC-Hemin in the 1st generation) supplemented with uracil) was inoculated with untransformed *S. cerevisiae* as a negative control. Plates were sealed and wrapped in Parafilm to prevent evaporation and incubated at 30 °C, 225 rpm and 80% relative humidity in a humidity shaker (Minitron-INFORS, Biogen, Spain). After 48 h, 160 μL of microplate expression medium YP-Hb (YP-EtOH in the 1st generation) was added to each well and the plates were incubated for a further 24 h. The plates (master plates) were centrifuged for 15 min at 3000 rpm at 4 °C (Eppendorf 5810R centrifuge with A-4-62 rotor, Germany) and they were duplicated with the help of a robot (Liquid Handler EVOFreedom-100, TECAN, Switzerland) by transferring 20 μL of supernatant into two replica plates: the acid activity plate (AA plate; activity at acid pH) and the basic activity plate (BA plate; activity at alkaline pH). Then, 180 μL of reaction mixture were added in each plate using a Multidrop robot (Multidrop Combi, Thermo Fischer Scientific, Vantaa, Finland). The reaction mixture for AA plates contained 100 mM citrate–phosphate buffer (pH 4.0), 2 mM ABTS and 0.1 mM H_2O_2. The reaction mixtures for BA plates contained 100 mM citrate–phosphate buffer (pH 6.0, 7.0 and 8.5 for 1st, 2nd and 3rd generation, respectively), 2 mM ABTS and 0.1 mM H_2O_2. The plates were stirred briefly and the absorption at 418 nm ($\varepsilon_{ABTS^{\cdot+}}$ = 36 000 M^{-1} cm^{-1}) was recorded in kinetic mode on a microplate reader (SPECTRAMax Plus 384, Molecular Devices, Sunnyvale, CA). The improvements in the alkaline range were calculated as the ratio between BA/AA plates and normalized to the parental type in the corresponding plate. To rule out false positives, three consecutive re-screenings were carried out (including the determination of pH activity and stability profiles and thermostabilities; see the ESI†). Production and purification of VP variants: VP variants were produced and purified as described in the ESI.†

2.3 Kinetic parameters

Kinetics were assayed with increasing substrate concentrations and fitted to a Michaelis–Menten model (steady-state enzyme kinetics) using as template a hyperbolic, single rectangular, two parameter mode. The catalytic efficiency (k_{cat}/K_m) was obtained by plotting turnover rates (s^{-1}) *vs.* substrate concentration and fitting it to a modified hyperbola with the function $f(x) = (ax)/[(1 + bx)]$, where a is the catalytic efficiency and b is $1/K_m$. The kinetics were measured with the following enzyme concentrations: 1.5–0.3 × 10^{-3} μM (for ABTS), 2 × 10^{-2} μM (for RB5), 2 × 10^{-2} μM (for Mn^{2+}) and 2.5 × 10^{-2} μM (for VA). The following molar extinction coefficients were used: ABTS, ε_{418} = 36 000 M^{-1} cm^{-1}; RB5, ε_{598} = 30 000 M^{-1} cm^{-1}; VA, ε_{310} = 9300 M^{-1} cm^{-1}; Mn^{3+}-tartrate, ε_{238}

Published on 14 June 2016. Downloaded by Centro de Investigaciones Biologicas (CIB) on 14/09/2016 13:11:33.

= 6500 M^{-1} cm^{-1}. Kinetics measurements for ABTS were performed in 100 mM citrate–phosphate–borate buffer from pH 3.0 to 8.0. Kinetics measurements for RB5 and VA were performed in 100 mM citrate–phosphate buffer (pH 3.5) and those for Mn^{2+} were in 100 mM sodium tartrate buffer (pH 5.0).

2.4 pH activity profiles

The activities of purified VP variants were measured in a range of pHs with different substrates. Appropriate enzyme dilutions were prepared for each case depending on the substrate. Substrate concentrations were adjusted to be below the inhibition threshold. The reaction mixtures contained 100 mM citrate–phosphate–borate buffer with pH values ranging from 2.0 to 10.0, 0.1 mM H_2O_2 and the following substrates: 2,6-DMP (5 mM), veratryl alcohol (30 mM), reactive black 5 (0.04 mM), guaiacol (20 mM), catechol (5 mM), sinapic acid (0.25 mM), syringaldazine (0.05 mM) and ABTS ([pH 2.0 to 4.0] 0.1 mM; [pH 5.0] 0.15 mM; [pH 6.0] 0.2 mM; [pH 7.0] 0.8 mM; [pH 8.0 to 10.0] 2.4 mM for BB-8; and [pH 2.0 to 6.0] 0.4 mM; [pH 7.0 to pH 9.0] 2.4 mM for 2-1B). The manganese and VA activities were performed in UV-star plates (Greiner Bio-One GmbH, Germany). The Mn^{2+} reaction mixtures were 100 mM tartrate buffer [pH 3.0 to 5.0], 60 mM manganese sulphate, and 0.1 mM H_2O_2. The activities were recorded from triplicate experiments on a plate reader using 200 μL of final volume per reaction (20 μL of purified enzyme plus 180 μL of reaction mixture). Specific activities were determined using the following molar extinction coefficients: ABTS, ε_{418} = 36 000 M^{-1} cm^{-1}; 2,6-DMP, ε_{469} = 27 500 M^{-1} cm^{-1}; RB5, ε_{598} = 30 000 M^{-1} cm^{-1}; VA, ε_{310} = 9300 M^{-1} cm^{-1}; guaiacol, ε_{470} = 26 600 M^{-1} cm^{-1}; catechol, ε_{392} = 1460 M^{-1} cm^{-1}; sinapic acid, ε_{312} = 16 700 M^{-1} cm^{-1}; syringaldazine, ε_{525} = 65 000 M^{-1} cm^{-1}; Mn^{3+}-tartrate, ε_{238} = 6500 M^{-1} cm^{-1}. Protein concentrations were spectrophotometrically measured with ${}_{VP}\varepsilon_{407nm}$ = 150 000 M^{-1} cm^{-1}.

2.5 Ultracentrifugation experiments

Sedimentation velocity (SV) assay: purified VPs were diluted in 100 mM citrate–phosphate–borate buffer (at pH 4.0 and pH 9.0) containing 250 mM NaCl, 10 mM $MgCl_2$, 1 mM EDTA and 100 mM glycerol. Samples were loaded (320 μL) into analytical ultra-centrifugation cells. The experiments were carried out at 48 000 RPM in an XL-I analytical ultracentrifuge (Beckman-Coulter Inc.) equipped with UV-vis absorbance and Rayleigh interference detection systems. Sedimentation profiles were recorded at 403 nm. Sedimentation coefficient distributions were calculated by least-squares boundary modelling of sedimentation velocity data using the continuous distribution $c(s)$ Lamm equation model as implemented by SEDFIT 14.1.[28] Experimental S values were corrected to standard conditions (water, 20 °C, and infinite dilution) using the program SEDNTERP[29] to get the corresponding standard S values ($S_{20,w}$). Sedimentation equilibrium (SE) assay: using the same experimental conditions as in the SV experiments, short column (90 μL) SE experiments were carried out at speeds ranging from 12 000 to 18 000 rpm and at 407 nm. After the last equilibrium scan, a high-speed centrifugation run (48 000 rpm) was done to estimate the corresponding baseline offsets. Weight-average buoyant molecular weights of protein were determined by fitting a single species model to the experimental data using the HeteroAnalysis program,[30] and corrected for solvent composition and temperature with the program SEDNTERP.[29]

2.6 Protein and homology modeling

The crystal structure of VPl2 from *P. eryngii* expressed in *E. coli* at 2.11 Å resolution (1 Å = 0.1 nm, PDB ID: 3FM4) was used to generate a model to map new mutations with the help of the PyMOL Molecular Visualization System (Schrödinger).

2.7 DNA sequencing

Plasmids containing the VP variants were sequenced on an ABI 3730 DNA Analyzer (Applied Biosystems) automatic sequencer at the Secugen (CIB, Madrid) using the following primers: RMLN; 3R-direct primer (5′-GTTCCATCATCGCGTTCG-3′); 5F-reverse primer (5′-GGATTCCTTTCTTCTTGG-3′) and RMLC.

3. Results and discussion

3.1 Engineering strategy

To obtain a VP that was active at basic pHs, the 2-1B VP variant we generated previously was subjected to directed evolution by error-prone PCR in combination with hybrid approaches (Fig. 1).

Using ABTS as the reducing substrate for the screening assay, the ratio of the activity at pH 4.0 to that at neutral/basic pH was used as the selection criterion in the evolution experiment. Thus, only clones that retained ≥80% of the enzyme's activity at pH 4.0, yet displayed enhanced activity at alkaline pH, were selected for further characterization. Indeed, we used this approach to gradually increase the selective pressure during the course of the directed evolution from pH 6.0 to 8.5, while widening the pH activity profile (Fig. 2A). The yeast microfermentation conditions and the expression of the mutant libraries in 96-well plates were also adjusted to guarantee the reliable detection of VP activity under such demanding conditions. These modifications mainly affected the composition of the medium (heme supply, carbon source) as well as the stirring conditions and oxygen availability (see the ESI† for details).

We planned to precisely control the evolutionary route by using low mutational loads, 1 to 3 nucleotide changes per round of evolution, coupled to *in vivo* recombination.[31] Three consecutive re-screenings were performed to determine the pH activity and stability profiles of the new variants (in the pH range of 2.0 to 10.0) as well as the T_{50} (the temperature at which the enzyme loses 50% of its initial activity after a 10

 This journal is © The Royal Society of Chemistry 2016

Published on 14 June 2016. Downloaded by Centro de Investigaciones Biologicas (CIB) on 14/09/2016 13:11:33.

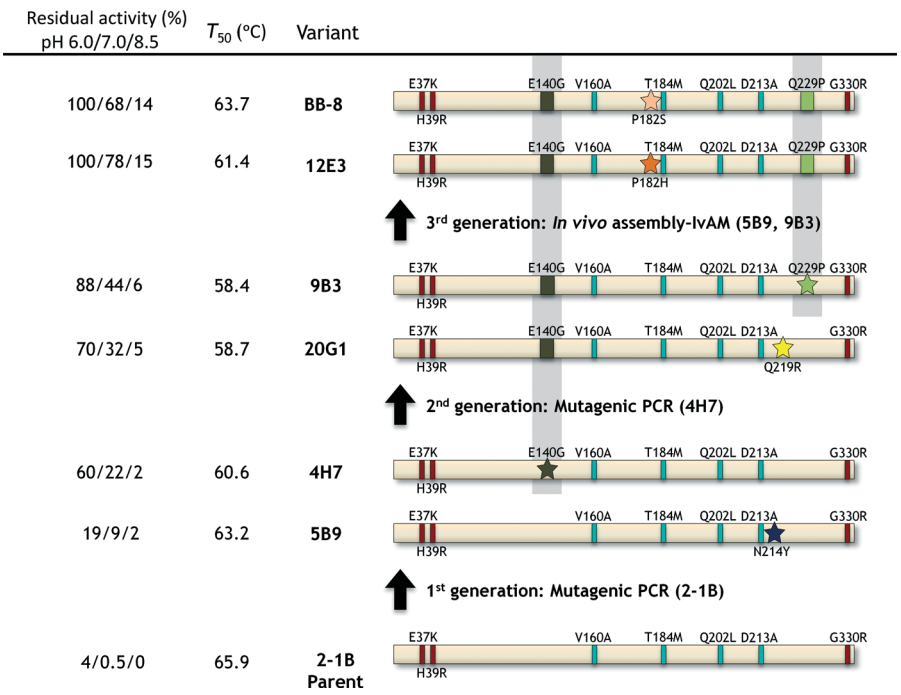

Fig. 1 Directed evolution of an alkaline VP. New mutations are depicted as stars and accumulated mutations as squares. Mutations from previous evolution campaigns[24] are shown as thin squares with the stabilizing mutational backbone in dark red. The method used for library creation and the parental types used for each generation are indicated. Residual activity (%) was calculated as the improvement in VP activity detected in *S. cerevisiae* supernatants for each mutant compared with the parental 2-1B at the corresponding pH. Measurements were made in quintuplicate with 2 mM ABTS and 0.1 mM H_2O_2 in 100 mM citrate–phosphate–borate buffer at different pHs. Thermostability (T_{50}) was estimated from the culture supernatants.

min incubation). After screening ~5000 clones in three rounds of directed evolution, the BB-8 mutant was obtained that carried the beneficial E140G, P182S and Q229P mutations.

This variant had nearly the same activity at pH 6.0 as that of the parental 2-1B variant at pH 4.0 (Fig. 2A), although unlike the 2-1B variant, the activity of BB-8 at a neutral/basic pH was readily detected. The drop in thermostability (T_{50}) identified in the first two rounds of evolution (from 66 to 58 °C, Fig. 1) was partly alleviated by including a stabilizing mutation, P182S, in the last generation, allowing BB-8 to recover ~5 °C. Given that the same position was mutated to different amino acids in two independent variants identified (12E3 and BB-8), we performed further saturation mutagenesis over this Pro182 residue. The best mutants obtained displayed a ~2-fold enhancement of activity at pH 8.0 over the original Pro182 (the 9B3 mutant from the 2nd generation). In all cases, substitution with polar residues (Tyr, Glu, His, Ser) produced similar thermostabilities, pH activity and stability profiles (Fig. 2B). Accordingly, BB-8 was selected for more exhaustive characterization.

3.2 Alkaline pH stabilization and hyperactivation

The wild-type VP ($_{wt}$VP), 2-1B and BB-8 mutants were produced, purified to homogeneity (Reinheitszahl value [Rz] [A_{407}/A_{280}], ≥2) and characterized spectroscopically and biochemically. Initially, the electronic absorption spectrum was recorded after incubating the enzymes for 72 h at pH 4.0 and 9.0 (Fig. 3A). At pH 4.0 (optimum pH for activity) the maximum absorbance of all VPs was in the Soret region (407 nm) and the two charge transference bands (CT2, 505 nm; CT1, 637 nm) were characteristic of Fe^{3+} in a high-spin (pentacoordinated) state. As observed previously,[25] the incubation of $_{wt}$VP at alkaline pH changed its spectroscopic features and these modifications were detectable even after a 1 min incubation (Fig. 3A, see inset in the first panel). The Soret maximum shifted from 407 to 413 nm and the CT bands faded, while two new shoulders arose at 532 and 565 nm that are characteristic of a low-spin (hexacoordinated and inactive) state.[32]

By contrast, the 2-1B and BB-8 mutants remained unaltered after incubation for 72 h at pH 9.0, showing a similar spectrum to that seen at pH 4.0, although with lower absorbance values. Given that both the parental 2-1B and the BB-8 mutant harbour the aforementioned stabilizing E37K-H39R-G330R backbone, they preserved the heme state (*i.e.* remaining in a pentacoordinated high-spin Fe^{3+}). In fact, the mutants were very stable in such an alkaline environment when compared to $_{wt}$VP. As such, the 2-1B and BB-8 variants retained or even increased their residual activity after incubation at pH 9.0 (see below), whereas $_{wt}$VP was fully inactive at this pH, as reported previously (Fig. 3B).[24,25] The spectroscopic changes and the poor stability of $_{wt}$VP at alkaline pH

Published on 14 June 2016. Downloaded by Centro de Investigaciones Biologicas (CIB) on 14/09/2016 13:11:33.

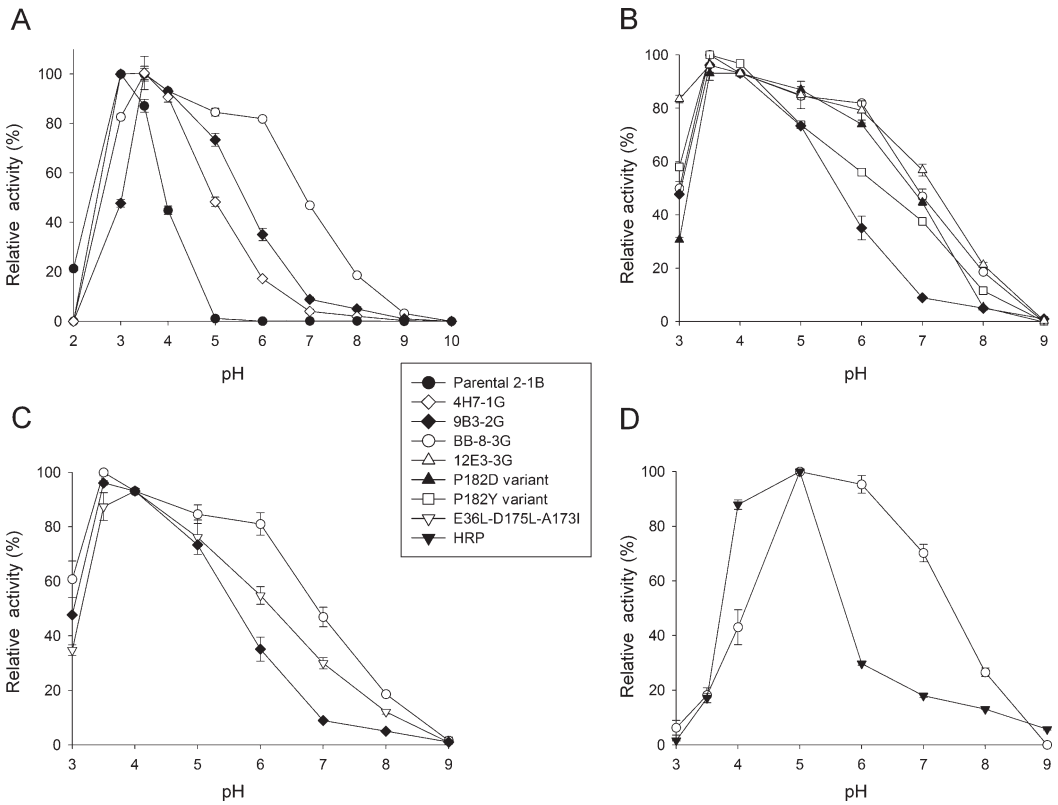

Fig. 2 Widening of the VP pH activity profile. (A) pH activity profiles for the parental 2-1B and the best mutant in each generation. Black circles, parental 2-1B; white diamonds, 4H7-1st generation; black diamonds, 9B3-2nd generation; white circles, BB-8-3rd generation. (B) pH profiles for selected mutants of saturation mutagenesis experiment at position 182. Black diamonds, 9B3-2nd generation (P182); white squares, P182Y mutant; black up triangles, P182D mutant; white up triangles, 12E3-3rd generation (P182H); white circles, BB-8-3rd generation (P182S). (C) pH activity profiles for E36L-D175L-A173I (white down triangles), 9B3-2nd generation (black diamonds) and BB-8-3rd generation (white circles) mutants. (D) pH profiles for HRP (black down triangles) and BB-8 (white circles). The concentrations of ABTS in (A)–(C) were adjusted to below the inhibitory threshold for each pH value (from pH 2.0 to 6.0, 0.4 mM and from pH 7.0 to 10.0, 2.4 mM for 2-1B; from pH 2.0 to 4.0, 0.1 mM; pH 5.0, 0.15 mM; pH 6.0, 0.2 mM; pH 7.0, 0.8 mM; pH 8.0 to 10.0, 2.4 mM for the other variants). In (D) we used 2 mM ABTS across the entire pH range as it is the concentration used for standard HRP assays. Activities were measured in 100 mM citrate–phosphate–borate buffer at different pHs with the [ABTS] indicated and 0.1 mM H_2O_2. The activity was normalized to the optimum activity value and the results shown are the means ± S.D. from three independent experiments.

are directly linked to the failure to attach the structural Ca^{2+}. Two specific ligands are involved in the coordination of Ca^{2+} (Ser170 for the proximal Ca^{2+}; Asp48 for the distal Ca^{2+}), lying adjacent to the corresponding proximal and distal His (His169 and His47, respectively). His169 is the 5th coordinating (axial) ligand of the heme group, while His47 is involved in the heterolytic cleavage of H_2O_2. It is well known that incubation at high temperature or pH provokes the release of structural Ca^{2+}, with the distal His47 concomitantly approximating to the heme and forming a bis-histidyl heme iron complex that is characteristic of a hexacoordinated low-spin inactive state.

We observed strong hyperactivation of VP mutants that was directly dependent on the length of incubation and the pH (Fig. 3B). Particularly, BB-8 was hyperactivated at pH 8.0 and 9.0, reaching a plateau after a 72 h incubation with a ~3-fold increase in residual activity. It is well known that enzyme hyperactivation can be associated with conformational changes that may occur after incubation at high temperatures or in the presence of organic co-solvents but we were not aware of such an effect by incubation at alkaline pHs. As enzyme hyperactivation might reflect a di/multimerization process, to rule out the possible formation of variant VP dimers at basic pHs, we carried out independent analytical ultracentrifugation experiments in which similar sedimentation coefficients of the mutants were obtained (sw(20,w) ~3 S) after incubation at acid (4.0) or basic pH (9.0). Further sedimentation equilibrium experiments corroborated the lack of dimerization, and a MW of ~34 000 Da for both enzymes was obtained at acid and basic pHs.

3.3 The pH activity profiles and the contribution of the Mn^{2+} binding site to direct substrate oxidation

The pH activity profiles of the purified variants were evaluated for different substrates, including some redox mediators and natural fungal metabolites at concentrations below their inhibitory thresholds (≤10-fold K_m value; Fig. 4). The low-redox potential substrates ABTS, sinapic acid and guaiacol can be oxidized at two different catalytic sites: the heme

 This journal is © The Royal Society of Chemistry 2016

Published on 14 June 2016. Downloaded by Centro de Investigaciones Biologicas (CIB) on 14/09/2016 13:11:33.

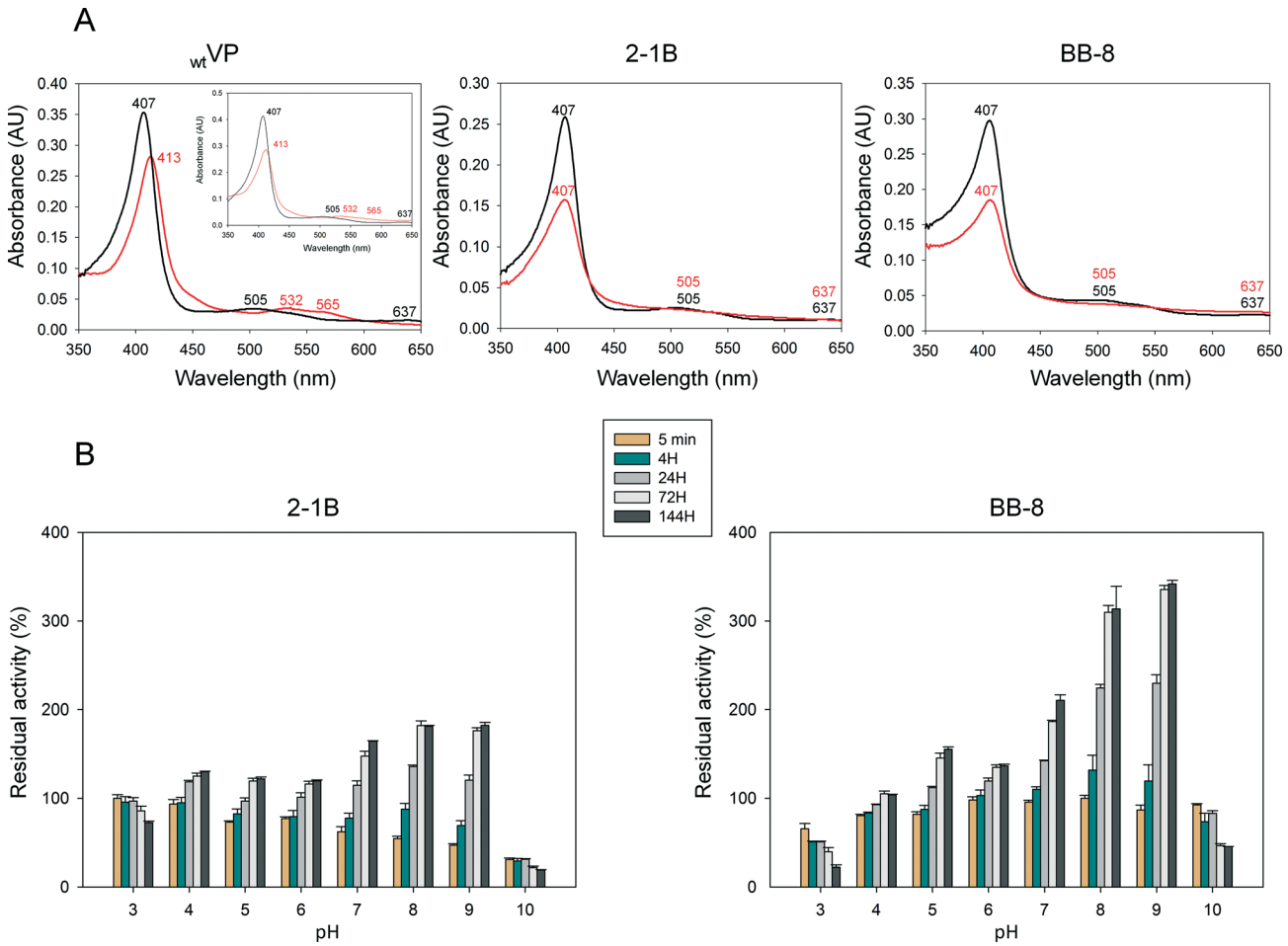

Fig. 3 VP stability at alkaline pHs. (A) Electronic absorption spectra of $_{wt}$VP and the 2-1B and BB-8 mutants. The UV-visible spectra after a 72 h incubation at pH 4.0 (black) and pH 9.0 (red) are shown. The graph for $_{wt}$VP includes an inset for the spectrum after 1 min of incubation at pH 4.0 (black) and pH 9.0 (red). (B) The pH stability profiles of the parental 2-1B and the BB-8 mutant. Enzyme samples were incubated in 100 mM citrate–phosphate–borate buffer at different pH values, and the residual activities were measured in 100 mM sodium tartrate buffer (pH 3.5) containing 2 mM ABTS and 0.1 mM H_2O_2. The results are the means ± S.D. from three independent experiments.

access channel (with low efficiency) and the catalytic Trp164 (with high efficiency). The pH profiles for these compounds were shifted and broadened towards the basic side, even detecting some activity at pH 9.0 where the parental 2-1B was inactive (Fig. 4A–C). Under acidic conditions, the veratryl alcohol (VA) and the reactive black five (RB5) high-redox potential substrates are oxidized at the Trp164 radical formed by LRET in both compounds I and II of VP after heme activation by H_2O_2.[33] However, at neutral or basic pH no oxidation of VA or RB5 was observed irrespective of the mutant tested (Fig. 4D and E). This is explained by the fact that the reduction potential of Trp164 radical decreases as the pH increases, with an estimated loss of 59 mV per unit of pH.[34] Thus, the LRET pathway from Trp164 to the heme is permanently cancelled at pH >5, diverting the oxidative route to the other two catalytic sites while suppressing the oxidation of high-redox potential compounds. It is noteworthy that the oxidation of Mn^{2+} to Mn^{3+} was drastically reduced for BB-8 (Fig. 4F), while the contribution of the Mn^{2+} binding site to the direct oxidation of low-redox potential substrates at alkaline pH (in the absence of oxidized Mn^{3+}) was evident for the first time within this enzyme superfamily. The Mn^{2+} site in VP is formed by the side chains of the three coordinating carboxylic residues (Glu36, Glu40 and Asp175), constituting a small channel that connects the protein surface to the internal propionate of the heme. In the 2-1B parental type, this catalytic site was partially suppressed for the oxidation of Mn^{2+} to Mn^{3+} due to the effect exerted by two of the mutations in the stabilizing backbone (E37K and H39R).[24,25] Moreover, the introduction of the P182S mutation in BB-8, situated in the neighbourhood of the Mn^{2+} site, negatively affected the kinetics for Mn^{2+} (see below). Conversely, we detected double slopes for the kinetics of ABTS at basic pHs, which must originate from the heme access channel and the Mn^{2+} binding site given that the catalytic Trp is inactive under such pH values.

To demonstrate this hypothesis, we inspected the structure of BB-8 and designed a triple mutant (E36L-D175L-A173I) in which the substrate cannot access the Mn^{2+} binding site (Fig. 5). As expected, the analysis of the pH activity

Published on 14 June 2016. Downloaded by Centro de Investigaciones Biologicas (CIB) on 14/09/2016 13:11:33.

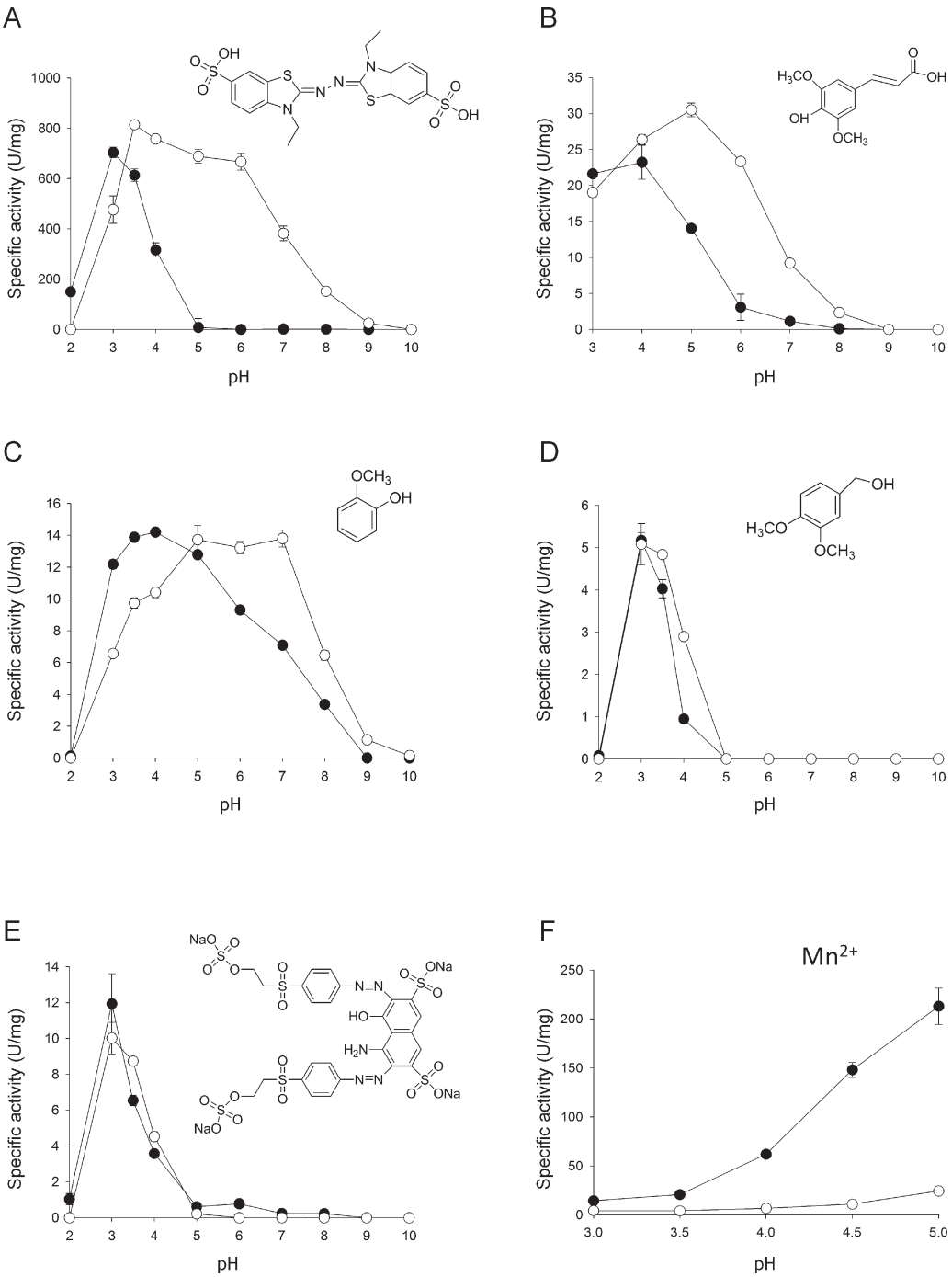

Fig. 4 pH Activity profiles. pH profiles for the parental 2-1B (black circles) and the BB-8 mutant (white circles) with ABTS (A), sinapic acid (B), guaiacol (C), VA (D), RB5 (E) and Mn^{2+} (F). Activities were measured in 100 mM citrate–phosphate–borate buffer at different pHs with a concentration of the substrate below their inhibitory threshold (see the ESI† for details) and 0.1 mM H_2O_2. VP activity was normalized to the optimum activity (U mg^{-1}) and the results shown are the means ± S.D. from three independent experiments.

profiles of BB-8 and the triple mutant confirmed the contribution of the Mn^{2+} site to the direct oxidation of ABTS at pH >6.0 (up to ~26%; Fig. 2C). We also included in these measurements the 9B3 mutant (from the 2nd generation) that lacked the P182S mutation of BB-8 to obtain a reliable breakdown of the activity at the heme channel and the Mn^{2+} site at basic pHs. While the difference between the triple mutant and 9B3 from pH >6 onwards represents the enhanced activity at the heme channel, the comparison between the E36L-D175L-A173I triple variant and BB-8 reflects that at the Mn^{2+} site. Our results are consistent with the data from an earlier rational and computational analysis of a short MnP that indicated the direct oxidation of ABTS at the Mn^{2+} site at acidic pHs.[35]

 This journal is © The Royal Society of Chemistry 2016

Published on 14 June 2016. Downloaded by Centro de Investigaciones Biologicas (CIB) on 14/09/2016 13:11:33.

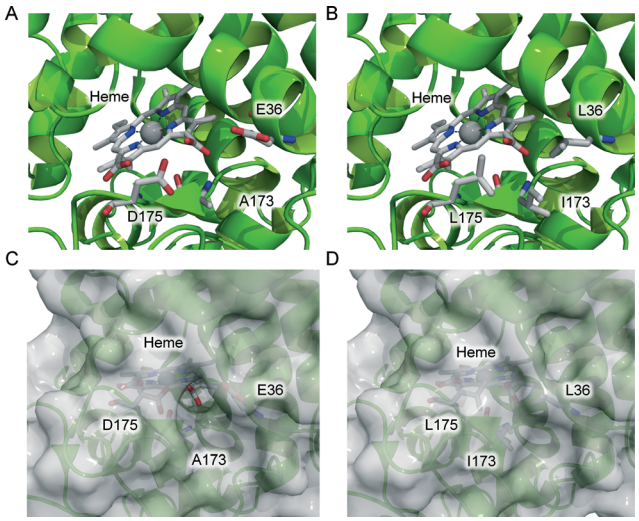

Fig. 5 Site-directed mutagenesis to block the Mn^{2+} binding site. The VP structure is shown as a green cartoon while the heme group and the residues targeted for mutagenesis are highlighted as sticks (CPK-colors), before (A) and after (B) mutagenesis to block the Mn^{2+} binding site. The bottom panel shows the protein topology in the surface mode before (C) and after (D) mutagenesis. Mutations modelled from PDB ID: 3FM4.

3.4 Kinetic parameters

Kinetic constants were assessed in the pH range from 3.5 to 8.0 (Table 1). The catalytic efficiency (k_{cat}/K_m) of BB-8 for ABTS was 5-fold higher than that of the parental 2-1B at pH 3.5. This large improvement was associated with the mutant's activity at alkaline pHs, even though the affinity and activity gradually declined (k_{cat}/K_m) as more basic pHs were reached. Still, the catalytic efficiency of BB-8 at pH 8.0 was higher than that of $_{wt}$VP at optimum pH, 3.5 (*i.e.* 1190 *vs.* 410 mM^{-1} s^{-1}, respectively).[24]

Encouraged by these results, we compared the pH activity profile of BB-8 to that of HRP (horseradish peroxidase). HRP is widely used in many analytical and biomedical applications (*e.g.*, to report biological activities linked to the production of H_2O_2, chemiluminiscence detection in western blots, *etc.*).[36] Our variant by far surpassed the activity of HRP from pH 5.0 onwards, offering an attractive solution for applications at basic pHs that require peroxidase activity (Fig. 2D). Finally, in terms of high-redox potential substrates, the kinetics for RB5 and VA were similar irrespective of the variant, while Mn^{2+} oxidation was almost completely suppressed in BB-8, with a 13-fold increase in the K_m (Table 2).

3.5 Structural analysis of mutations

The mutations found in BB-8 were mapped to the VP crystal structure (Fig. 6). The E140G mutation introduced in the first round of evolution exerted the strongest improvement in the whole study, with a ~44-fold increase in activity at pH 7.0, opening the way for evolution at alkaline pH (Fig. 1). This mutation is located at the entry to the heme access channel (Fig. 6A and B) and it seems to be the main residue responsible for the improved kinetics. Upon mutation, the heme channel is widened, facilitating the entrance and exit of bulky substrates, thereby favouring catalysis. Indeed, the gradual decrease in substrate affinity associated with higher pH values was alleviated by the E140G substitution, associated with a ~4-fold better K_m (Table 1) that enabled BB-8 to work at pH 6.0 with similar efficiency to the parental 2-1B variant at pH 3.5. Our results agree well with a previous rational experiment where the same mutation was introduced into VP, increasing catalytic efficiency by 4-fold.[13] Unfortunately, the E140G mutant in that study did not show any activity at pH >4 since it lacked the stabilizing E37K-H39R-G330R backbone that protects the enzyme against Ca^{2+} leakage. The Q229P mutation lies in a sensitive region close to the proximal Ca^{2+}. Inspection of the model suggests that this mutation affects the distance to the H-bonded Gly216, influencing the main loop of the heme access channel and modifying catalysis (Fig. 6C and D). The P182S mutation introduced in the last generation fostered activity at alkaline pHs and recovered most of the lost thermostability (~5 °C). This mutation lies in a rather labile region, between the heme access channel and in the vicinity of the Mn^{2+} binding site (Fig. 6E and F). It is likely that Pro182 exerts a destabilizing effect under alkaline conditions given that proline residues are generally indicators of protein destabilization under harsh conditions.[37] Indeed, all the mutants derived from the saturation mutagenesis at Pro182 had polar side chains introduced, providing reinforcement in this region by establishing new contacts with surrounding residues.

Moreover, potential reshaping of the Mn^{2+} binding site after mutation for the direct oxidation of substrates in the absence of Mn^{2+} cannot be ruled out. Molecular docking simulations with ABTS at the Mn^{2+} site indicates that a new

Table 1 Kinetic parameters with ABTS at different pH values

Mutant	Kinetic constants	pH 8.0	pH 7.0	pH 6.0	pH 5.0	pH 4.0	pH 3.5
BB-8	K_m (mM)	0.154 ± 0.018	0.078 ± 0.004	0.039 ± 0.005	0.013 ± 0.002	0.011 ± 0.002	0.0078 ± 0.002
	k_{cat} (s^{-1})	184 ± 6	460 ± 6	810 ± 30	840 ± 30	920 ± 30	990 ± 40
	k_{cat}/K_m (mM^{-1} s^{-1})	1190 ± 110	5910 ± 270	20 500 ± 2000	64 000 ± 9600	79 000 ± 11 700	126 000 ± 26 500
2-1B	K_m (mM)	n.m.	n.m.	n.m.	n.m.	0.17 ± 0.01	0.034 ± 0.004
	k_{cat} (s^{-1})	n.m.	n.m.	n.m.	n.m.	670 ± 20	850 ± 40
	k_{cat}/K_m (mM^{-1} s^{-1})	n.m.	n.m.	n.m.	n.m.	3900 ± 200	25 000 ± 2100

Kinetics were estimated in 100 mM citrate–phosphate–borate buffer containing 0.1 mM H_2O_2 at different pH values; n.m., not measurable.

Published on 14 June 2016. Downloaded by Centro de Investigaciones Biologicas (CIB) on 14/09/2016 13:11:33.

Table 2 Kinetic parameters with Mn^{2+}, VA and RB5

Mutant	Kinetic constants	Mn^{2+}	VA	RB5
BB-8	K_m (mM)	56 ± 10	24.7 ± 1.9	0.021 ± 0.001
	k_{cat} (s^{-1})	70 ± 8	21.3 ± 0.9	20.4 ± 0.4
	k_{cat}/K_m (mM^{-1} s^{-1})	1.25 ± 0.08	0.86 ± 0.02	950 ± 30
2-1B	K_m (mM)	4.3 ± 0.3	7.14 ± 0.6	0.0055 ± 0.0006
	k_{cat} (s^{-1})	98 ± 2	2.9 ± 0.1	9.4 ± 0.4

Kinetics were estimated in 100 mM citrate–phosphate–borate buffer at pH 3.5 containing 0.1 mM H_2O_2 and for Mn^{2+} in 100 mM sodium tartrate buffer at pH 5.0.

H-bond between one of the SO^{3-} moieties of ABTS and Ser182 may more adequately orientate and direct substrate oxidation through the internal heme propionate (Fig. S1, ESI†). This data agrees well with the changes observed in the aforementioned E36L-D175L-A173I triple mutant in which the use of the Mn^{2+} site for Mn^{2+} oxidation to Mn^{3+} was rescinded. Finally, and to estimate the degree of conservation of the mutated positions, we generated a multiple sequence alignment (MSA) with an array of the most representative ligninolytic peroxidases (Fig. S2, ESI†). Interestingly, E140 and Q229 together with two of the residues in the stabilizing backbone (E37, H39) are highly conserved within this enzyme superfamily. Hence, introducing these mutations into other ligninolytic peroxidases may also influence alkaline activation/stabilization.

4. Conclusions

High-redox potential peroxidases are the product of millions of years of adaptation to achieve lignin combustion at acidic pHs. In particular, VPs are hybrid proteins that combine the best catalytic attributes of GPs, LiPs and MnPs. Very recently, we reconstructed several ancestral nodes of ligninolytic peroxidases which have been resurrected and functionally expressed in bacteria and yeast (unpublished material). All these nodes are suitable moulds that can be used as templates for protein engineering in which hot-spot mutations could be introduced, such as those discovered here or in other directed evolution campaigns.[24,38] Thus, by defining the different mechanisms of action used by VPs, we help answer key questions regarding the natural evolution of ligninolytic peroxidases, particularly as VPs were recently postulated as the evolutionary link between MnPs and LiPs.[6]

Finally, we have taken the VP from its natural biological context to make it active at alkaline pHs for the first time. Indeed, this alkaline VP is the result of the synergy between a

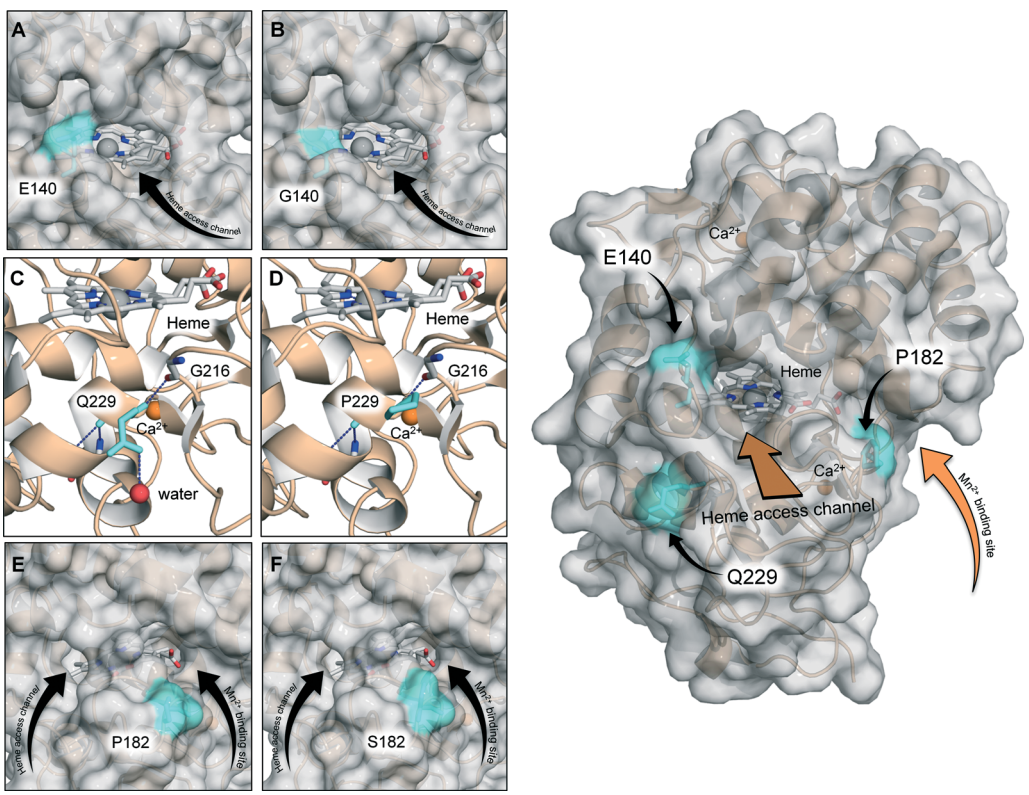

Fig. 6 Location of the mutations in alkaline VP. The mutations are highlighted in blue as sticks, the heme group is in the CPK stick mode and the structural calcium is shown as orange spheres. The protein surface is shown in transparent grey and the protein's secondary structures as a wheat cartoon. Orange arrows represent the substrate inlets. (A and B) E140G mutation, with the black arrow indicating the heme access channel. (C and D) The Q229P mutation, with the dotted blue lines showing the interactions with surrounding residues and the red sphere representing a water molecule. (E and F) P182S mutation, with black arrows showing the access to the heme channel and the Mn^{2+} site. Mutations modelled on PDB ID: 3FM4.

 This journal is © The Royal Society of Chemistry 2016

Published on 14 June 2016. Downloaded by Centro de Investigaciones Biologicas (CIB) on 14/09/2016 13:11:33.

stabilizing backbone that maintains the integrity of the heme by avoiding calcium leakage, and mutations that allow the VP to act at basic pHs by enhancing its substrate affinity and permitting direct oxidation at the Mn^{2+} site. This biocatalyst could be tested in applications at neutral/basic pHs, ranging from organic synthesis, biomedicine, pulp biobleaching to bioremediation, as well as for the engineering of a fully consolidated microbe to produce biofuels and chemicals.[2,39]

Acknowledgements

We thank Dr Juan Roman Luque-Ortega (Laboratory of Analytical Ultracentrifugation and Macromolecular Interactions, CIB-CSIC, Madrid) for assisting in AUC assays. This research was supported by the European Commission project FP7-KBBE-2013-7-613549-INDOX, the COST-Action CM1303 and by the Spanish government (grants: BIO2013-43407-R-DEWRY and CAMBIOS-RTC-2014-1777-3).

Notes and references

1 M. E. Himmel, S. Y. Ding, D. K. Johnson, W. S. Adney, M. R. Nimlos, J. W. Brady and T. D. Foust, *Science*, 2007, **315**, 804–807.
2 M. Alcalde, *Trends Biotechnol.*, 2015, **33**, 155–162.
3 A. T. Martínez, F. J. Ruiz-Dueñas, M. J. Martínez, J. C. del Río and A. Gutiérrez, *Curr. Opin. Biotechnol.*, 2009, **20**, 348–357.
4 E. Garcia-Ruiz, D. M. Mate, D. Gonzalez-Perez, P. Molina-Espeja, S. Camarero, A. T. Martínez, A. O. Ballesteros and M. Alcalde, in *Cascade Biocatalysis: Integrating Stereoselective and Environmentally Friendly Reactions*, ed. S. Riva and W. D. Fessner, Wiley-VCH Verlag GmbH & Co. KGaA, Weinheim, Germany, 2014, ch. 1, pp. 1–18.
5 K. E. Hammel and D. Cullen, *Curr. Opin. Plant Biol.*, 2008, **11**, 349–355.
6 D. Floudas, M. Binder, R. Riley, K. Barry, R. A. Blanchette, B. Henrissat, A. T. Martínez, R. Otillar, J. W. Spatafora, J. S. Yadav, A. Aerts, I. Benoit, A. Boyd, A. Carlson, A. Copeland, P. M. Coutinho, R. P. de Vries, P. Ferreira, K. Findley, B. Foster, J. Gaskell, D. Glotzer, P. Górecki, J. Heitman, C. Hesse, C. Hori, K. Igarashi, J. J. Jurgens, N. Kallen, P. Kersten, A. Kohler, U. Kües, T. K. A. Kumar, A. Kuo, K. LaButti, L. F. Larrondo, E. Lindquist, A. Ling, V. Lombard, S. Lucas, T. Lundell, R. Martin, D. J. McLaughlin, I. Morgenstern, E. Morin, C. Murat, L. G. Nagy, M. Nolan, R. A. Ohm, A. Patyshakuliyeva, A. Rokas, F. J. Ruiz-Dueñas, G. Sabat, A. Salamov, M. Samejima, J. Schmutz, J. C. Slot, F. St John, J. Stenlid, H. Sun, S. Sun, E. Syed, A. Tsang, A. Wiebenga, D. Young, A. Pisabarro, D. C. Eastwood, F. Martin, D. Cullen, I. V. Grigoriev and D. Hibbett, *Science*, 2012, **336**, 1715–1719.
7 M. Hofrichter, R. Ullrich, M. J. Pecyna, C. Liers and T. Lundell, *Appl. Microbiol. Biotechnol.*, 2010, **87**, 871–897.
8 M. Zámocký, B. Gasselhuber, P. G. Furtmüller and C. Obinger, *Cell. Mol. Life Sci.*, 2014, **71**, 4681–4696.
9 F. J. Ruiz-Dueñas, M. Morales, E. García, Y. Miki, M. J. Martínez and A. T. Martínez, *J. Exp. Bot.*, 2009, **60**, 441–452.
10 F. J. Ruiz-Dueñas and A. T. Martínez, *Microb. Biotechnol.*, 2009, **2**, 164–177.
11 M. Pérez-Boada, F. J. Ruiz-Dueñas, R. Pogni, R. Basosi, T. Choinowski, M. J. Martínez, K. Piontek and A. T. Martínez, *J. Mol. Biol.*, 2005, **354**, 385–402.
12 F. J. Ruiz-Dueñas, M. Morales, M. J. Mate, A. Romero, M. J. Martínez, A. T. Smith and A. T. Martínez, *Biochemistry*, 2008, **47**, 1685–1695.
13 M. Morales, M. J. Mate, A. Romero, M. J. Martínez, A. T. Martínez and F. J. Ruiz-Dueñas, *J. Biolumin. Chemilumin.*, 2012, **287**, 41053.
14 V. Sáez-Jimenez, M. C. Baratto, R. Pogni, J. Rencoret, A. Gutierrez, J. I. Santos, A. T. Martínez and F. J. Ruiz-Dueñas, *J. Biolumin. Chemilumin.*, 2015, **290**, 23201–23213.
15 C. Regalado, B. E. García-Almendárez and M. A. Duarte-Vázquez, *Phytochem. Rev.*, 2004, **3**, 243–256.
16 A. T. Martínez, in *Industrial Enzymes: Structure, Function and Applications*, ed. J. Polaina and A. P. MacCabe, Springer, Berlin, 2007, ch. 27, pp. 475–486.
17 S. Sakai, Y. Yamada, T. Zenke and K. Kawakami, *J. Mater. Chem.*, 2009, **19**, 230–235.
18 P. Khan, D. Idrees, M. A. Moxley, J. A. Corbett, F. Ahmad, G. von Figura, W. S. Sly, A. Waheed and M. I. Hassan, *Appl. Biochem. Biotechnol.*, 2014, **173**, 333–355.
19 T. A. Lú–Chau, F. J. Ruiz-Dueñas, S. Camarero, G. Feijoo, M. J. Martínez, J. M. Lema and A. T. Martínez, *Bioprocess Biosyst. Eng.*, 2004, **26**, 287–293.
20 J. Verdin, R. Pogni, A. Baeza, M. C. Baratto, R. Basosi and R. Vázquez-Duhalt, *Biophys. Chem.*, 2006, **121**, 163–170.
21 G. Nie and S. D. Aust, *Arch. Biochem. Biophys.*, 1997, **337**, 225–231.
22 G. R. J. Sutherland, L. S. Zapanta, M. Tien and S. D. Aust, *Biochemistry*, 1997, **36**, 3654–3662.
23 S. J. George, M. Kvaratskhelia, M. J. Dilworth and R. N. F. Thorneley, *Biochem. J.*, 1999, **344**, 237–244.
24 E. Garcia-Ruiz, D. Gonzalez-Perez, F. J. Ruiz-Dueñas, A. T. Martínez and M. Alcalde, *Biochem. J.*, 2012, **441**, 487–498.
25 V. Sáez-Jimenez, S. Acebes, E. Garcia-Ruiz, A. Romero, V. Guallar, M. Alcalde, F. J. Medrano, A. T. Martinez and F. J. Ruiz-Dueñas, *Biochem. J.*, 2016, DOI: 10.1042/BCJ20160248, in press.
26 M. Zumárraga, S. Camarero, S. Shleev, A. Martínez-Arias, A. Ballesteros, F. J. Plou and M. Alcalde, *Proteins*, 2008, **71**, 250–260.
27 M. Alcalde, in *In Vitro Mutagenesis Protocols: Methods in Molecular Biology*, ed. J. Braman, Springer-Humana Press, Totowa, N. J., third edn., 2010, ch. 1, pp. 3–14.
28 P. Schuck, *Biophys. J.*, 2000, **78**, 1606–1609.
29 T. M. Laue, B. D. Shah, T. M. Ridgeway and S. L. Pelletier, in *Analytical ultracentrifugation in biochemistry and polymer science*, ed. S. E. Harding, A. J. Rowe and J. C. Horton, The Royal Society of Chemistry, Cambridge, UK, 1992, pp. 90–125.
30 J. L. Cole, *Methods Enzymol.*, 2004, **384**, 212–232.

Published on 14 June 2016. Downloaded by Centro de Investigaciones Biologicas (CIB) on 14/09/2016 13:11:33.

31 D. Gonzalez-Perez, E. Garcia-Ruiz and M. Alcalde, *Bioeng. Bugs.*, 2012, **3**, 172–177.
32 H. L. Youngs, P. Moënne-Loccoz, T. M. Loehr and M. H. Gold, *Biochemistry*, 2000, **39**, 9994–10000.
33 F. J. Ruiz-Dueñas, R. Pogni, M. Morales, S. Giansanti, M. J. Mate, A. Romero, M. J. Martínez, R. Basosi and A. T. Martínez, *J. Biolumin. Chemilumin.*, 2009, **284**, 7986–7994.
34 O. B. Morozova and A. V. Yurkovskaya, *J. Phys. Chem. B*, 2015, **119**, 140–149.
35 E. Fernández-Fueyo, S. Acebes, F. J. Ruiz-Dueñas, M. J. Martínez, A. Romero, F. J. Medrano, V. Guallar and A. T. Martínez, *Acta Crystallogr., Sect. D: Biol. Crystallogr.*, 2014, **70**, 3253–3265.
36 F. W. Krainer and A. Glieder, *Appl. Microbiol. Biotechnol.*, 2015, **99**, 1611–1625.
37 R. Verma, T. S. Wong, U. Schwaneberg and D. Roccatano, Methods in Molecular Biology, in *Directed evolution Library Creation: Methods and Protocols*, ed. E. M. J. Gillam, J. N. Copp and D. F. Ackerley, Springer, New York, second edn., 2014, ch. 19, pp. 279–290.
38 D. Gonzalez-Perez, E. Garcia-Ruiz, F. J. Ruiz-Dueñas, A. T. Martinez and M. Alcalde, *ACS Catal.*, 2014, **4**, 3891–3901.
39 A. T. Martínez, F. J. Ruiz-Dueñas, A. Gutiérrez, J. C. del Río, M. Alcalde, C. Liers, R. Ullrich, M. Hofrichter, K. Scheibner, L. Kalum, J. Vind and H. Lund, *Biofuels, Bioprod. Biorefin.*, 2014, **8**, 819–835.

 This journal is © The Royal Society of Chemistry 2016

Electronic Supplementary Material (ESI) for Catalysis Science & Technology.
This journal is © The Royal Society of Chemistry 2016

Alkaline versatile peroxidase by directed evolution

David Gonzalez-Perez[a], Ivan Mateljak[a], Eva Garcia-Ruiz[b], Francisco J. Ruiz-Dueñas[c], Angel T. Martinez[c] and Miguel Alcalde[a*]

[a]Department of Biocatalysis, Institute of Catalysis, CSIC, 28049 Madrid, Spain.

[b]Department of Chemical and Biomolecular Engineering, University of Illinois at Urbana-Champaign, Urbana, IL 61801, USA.

[c]Center for Biological Investigations, CSIC, Ramiro de Maeztu 9, 28040 Madrid, Spain.

[*]Corresponding author: Miguel Alcalde, Department of Biocatalysis, Institute of Catalysis, CSIC, Cantoblanco, 28049 Madrid, Spain. Phone: +34 915854806; Fax: +34 915854760; malcalde@icp.csic.es.

Contents:

Fig. S1. Molecular Docking for ABTS at the Mn^{2+} site
Fig. S2. MSA of representative ligninolytic peroxidases.
Supplemental experimental procedures

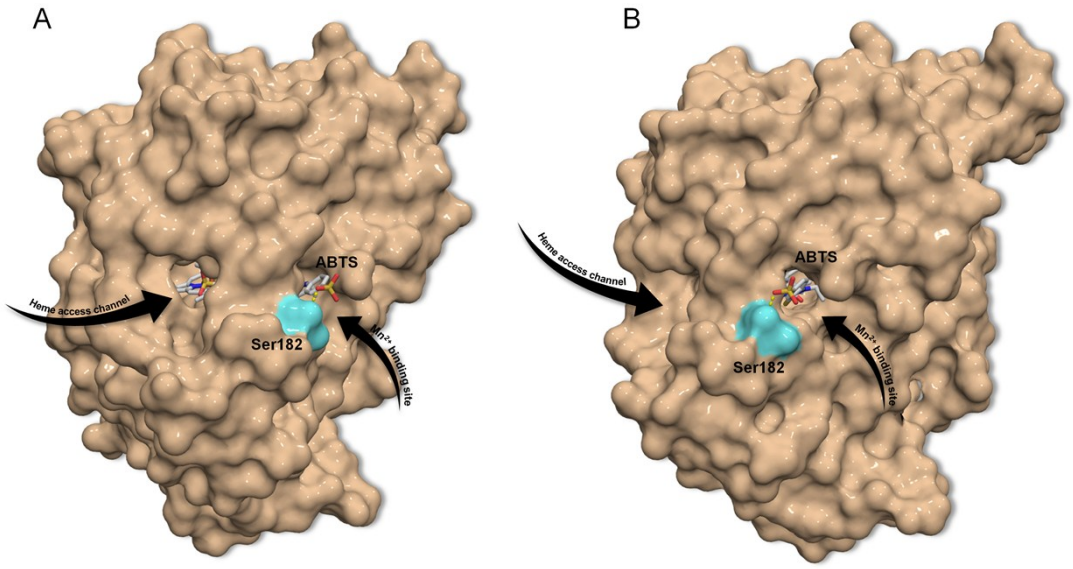

Fig. S1 Molecular Docking for ABTS at the Mn^{2+} site.

The protein is shown in the surface mode, the heme cofactor and ABTS are highlighted as stick models (CPK colors). The hydrogen bond between the SO^{3-} group of ABTS and Ser182 is represented as a yellow dash. The PDB file used for molecular docking was 3FKG. (**A**) Front view. (**B**) Side view.

Multiple structural alignment (MSA)

```
                                                                E37K  H39R
AURDE-GP11          ----RPAASVCADGVTTVNNPQCCFWANVRDRFINEIFL-GVCQENVHSLVRIAFHDAIG        55
PHLRA-MnP2          -------KTTCSNG-VVVPDAVCCDFVPLASALQSEVLM-GDCGEDAHELVRLIFHDAIA        51
PHACH-MnP1          --------AVCPDG-TRVSHAACCAFIPLAQDLQETIFQ-NECGEDAHEVIRLTFHDAIA        50
BJEAD-LiP           ---AIIKRVACPDGRHTAINAACCNLFTVRDDIQRNMFDGGKCNDIAHQALRLTFHDAVA        57
PHLRA-LiP3          --ASVTRRATCPDG-TQLMNAECCALLAVRDDLQNNMFN-NECGDEAHEALRLTFHDAIA        56
PHACH-LiPH8         --------ATCSNG-KTVGDASCCAWFDVLDDIQQNLFHGGQCGAEAHESIRLVFHDSIA        51
PLEOS-MnP4          ---VPAHRAKCSKG-RTASNDACCVWFDVLDDIQENLFDGGECGEEVHESLRLTFHDAIG        56
BJEAD-VP            ---AITRRVACPDGVNTATNAACCALFAVRDDIQQNLFDGGECGEEVHESLRLTFHDAIG        57
BB8-PLEER-VP        --------ATCDDG-RTTANAACCILFPILDDIQENLFDGAQCGEKVRESLRLTFHDAIG        51
PLEOS-MnP5          -VSLPQKRATCAGG-QVTANAACCVLFPLMEDLQKNLFDDGACGEDAHEALRLTFHDAIG        58
PLEOS-VP3           -VTLPQKRATCAGG-QVTANAACCVLFPILEDLQQNLFDGGECGEEVHESLRLTFHDAIG        58
Consensus                     *  *     .  **    : . :   .     *   .:. :*: ***::.

AURDE-GP11          FSLTD----PSKGGGADGSIIMFGDTELNFHANEGIDFITAFLQPFADTVG-VTYGDAIQ        110
PHLRA-MnP2          ISQSMG---PSAGGGADGSMLIFPTVEPAFFPNLGIADSVNNLIPFLSQFPTISAGDLVQ        108
PHACH-MnP1          ISRSQG---PKAGGGADGSMLLFPTVEPNFSANNGIDDSVNNLIPFMQKHNTISAADLVQ        107
BJEAD-LiP           FSPALEAEGKFGGNGADGSIITFGNIETNFHPNIGLDEIVEIEKPFIARHN-MTPGDFLH        116
PHLRA-LiP3          ISPAMEATGQFGGGGADGSIMIFSDIETKFHPNIGLDEVVESFRPFQQRSG-MGVADFIQ        115
PHACH-LiPH8         ISPAMEAQGKFGGGGADGSIMIFDDIETAFHPNIGLDEIVKLQKPFVQKHG-VTPGDFIA        110
PLEOS-MnP4          FSPALTRQGKFGGGGADGSIMLFSDIETNFAANNGVDDIVEQQKPIAIKHQ-VSFGDFIQ        115
BJEAD-VP            ISPSIAATGKFGGGGADGSIMIFDDIEPNFHANNGVDEIINAQKPFVAKHN-MTAGDFIQ        116
BB8-PLEER-VP        FSPTLG-----G-GGADGSIIAFDTIETNFPANAGIDEIVSAQKPFVAKHN-ISAGDFIQ        104
PLEOS-MnP5          FSPSRG-----VMGGADGSVITFSDTEVNFPANLGIDEIVEAEKPFLARHN-ISAGDLVH        112
PLEOS-VP3           FSPTKG-----G-GGADGSVLTFSDPEVNFPANLGIDEIVEAQKPFLARHN-ISAGDLVQ        111
Consensus           :* :          *****:: .   *  *  * *:        *:      :  .* :
```

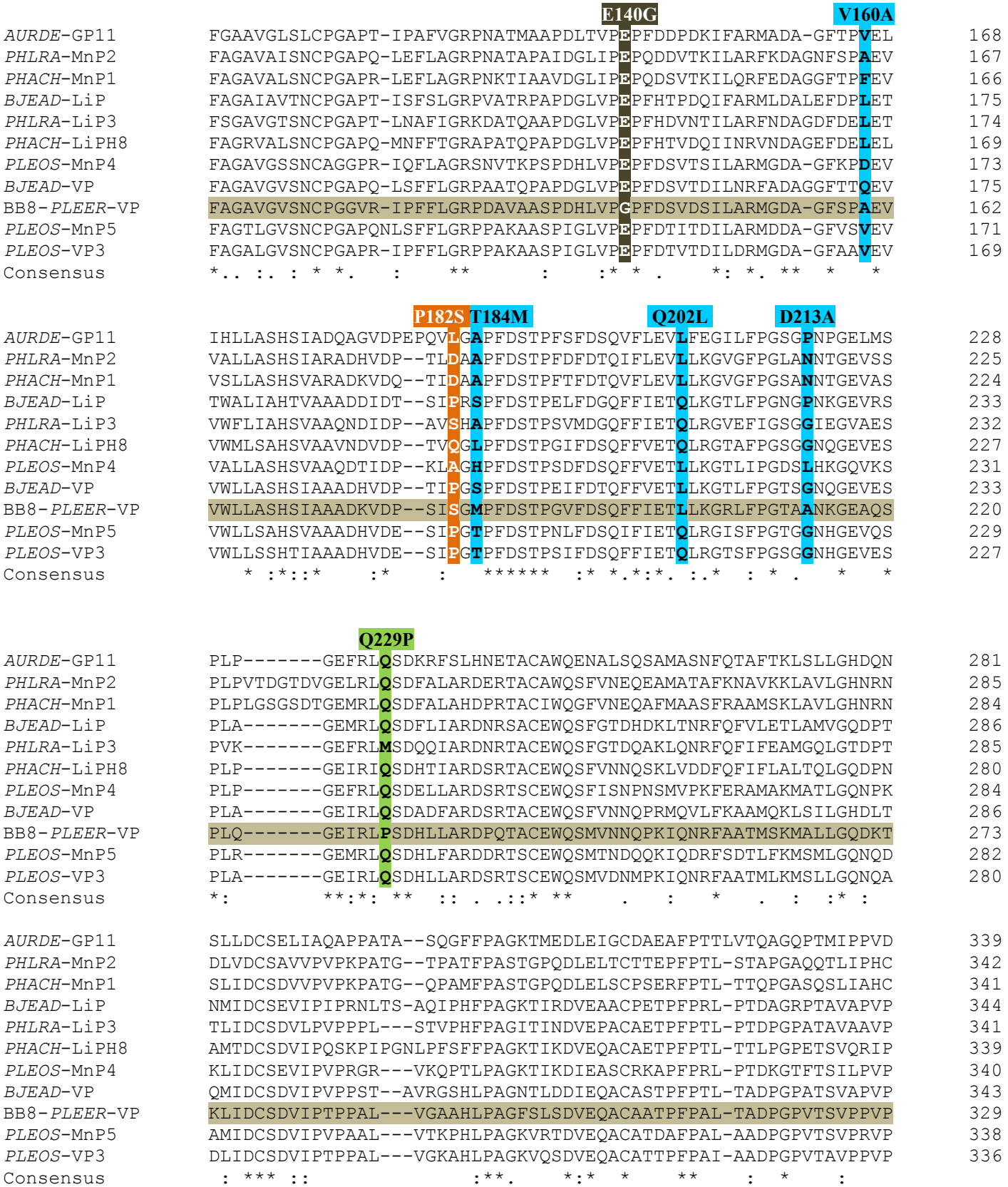
E140G
V160A
P182S
T184M
Q202L
D213A
Q229P
AURDE-GP11 FGAAVGLSLCPGAPT-IPAFVGRPNATMAAPDLTVPEPFDDPDKIFARMADA-GFTPVEL 168
PHLRA-MnP2 FAGAVAISNCPGAPQ-LEFLAGRPNATAPAIDGLIPEPQDDVTKILARFKDAGNFSPAEV 167
PHACH-MnP1 FAGAVALSNCPGAPR-LEFLAGRPNKTIAAVDGLIPEPQDSVTKILQRFEDAGGFTPFEV 166
BJEAD-LiP FAGAIAVTNCPGAPT-ISFSLGRPVATRPAPDGLVPEPFHTPDQIFARMLDALEFDPLET 175
PHLRA-LiP3 FSGAVGTSNCPGAPT-LNAFIGRKDATQAAPDGLVPEPFHDVNTILARFNDAGDFDELET 174
PHACH-LiPH8 FAGRVALSNCPGAPQ-MNFFTGRAPATQPAPDGLVPEPFHTVDQIINRVNDAGEFDELEL 169
PLEOS-MnP4 FAGAVGSSNCAGGPR-IQFLAGRSNVTKPSPDHLVPEPFDSVTSILARMGDA-GFKPDEV 173
BJEAD-VP FAGAVGVSNCPGAPQ-LSFFLGRPAATQPAPDGLVPEPFDSVTDILNRFADAGGFTTQEV 175
BB8-PLEER-VP FAGAVGVSNCPGGVR-IPFFLGRPDAVAASPDHLVPGPFDSVDSILARMGDA-GFSPAEV 162
PLEOS-MnP5 FAGTLGVSNCPGAPQNLSFFLGRPPAKAASPIGLVPEPFDTITDILARMDDA-GFVSVEV 171
PLEOS-VP3 FAGALGVSNCPGAPR-IPFFLGRPPAKAASPIGLVPEPFDTVTDILDRMGDA-GFAAVEV 169
Consensus *.. :. : * *. : ** : :* * . *: *. ** * *
AURDE-GP11 IHLLASHSIADQAGVDPEPQVLGAPFDSTPFSFDSQVFLEVLFEGILFPGSGPNPGELMS 228
PHLRA-MnP2 VALLASHSIARADHVDP--TLDAAPFDSTPFDFDTQIFLEVLLKGVGFPGLANNTGEVSS 225
PHACH-MnP1 VSLLASHSVARADKVDQ--TIDAAPFDSTPFTFDTQVFLEVLLKGVGFPGSANNTGEVAS 224
BJEAD-LiP TWALIAHTVAAADDIDT--SIPRSPFDSTPELFDGQFFIETQLKGTLFPGNGPNKGEVRS 233
PHLRA-LiP3 VWFLIAHSVAAQNDIDP--AVSHAPFDSTPSVMDGQFFIETQLRGVEFIGSGGIEGVAES 232
PHACH-LiPH8 VWMLSAHSVAAVNDVDP--TVQGLPFDSTPGIFDSQFFVETQLRGTAFPGSGGNQGEVES 227
PLEOS-MnP4 VALLASHSVAAQDTIDP--KLAGHPFDSTPSDFDSQFFVETLLKGTLIPGDSLHKGQVKS 231
BJEAD-VP VWLLASHSIAAADHVDP--TIPGSPFDSTPEIFDTQFFVETLLKGTLFPGTSGNQGEVES 233
BB8-PLEER-VP VWLLASHSIAAADKVDP--SISGMPFDSTPGVFDSQFFIETLLKGRLFPGTAANKGEAQS 220
PLEOS-MnP5 VWLLSAHSVAAADHVDE--SIPGTPFDSTPNLFDSQIFIETQLRGISFPGTGGNHGEVQS 229
PLEOS-VP3 VWLLSSHTIAAADHVDE--SIPGTPFDSTPSIFDSQFFIETQLRGTSFPGSGGNHGEVES 227
Consensus * :*::* :* : ****** :* *.*:*. :.* : * . * *
AURDE-GP11 PLP-------GEFRLQSDKRFSLHNETACAWQENALSQSAMASNFQTAFTKLSLLGHDQN 281
PHLRA-MnP2 PLPVTDGTDVGELRLQSDFALARDERTACAWQSFVNEQEAMATAFKNAVKKLAVLGHNRN 285
PHACH-MnP1 PLPLGSGSDTGEMRLQSDFALAHDPRTACIWQGFVNEQAFMAASFRAAMSKLAVLGHNRN 284
BJEAD-LiP PLA-------GEMRLQSDFLIARDNRSACEWQSFGTDHDKLTNRFQFVLETLAMVGQDPT 286
PHLRA-LiP3 PVK-------GEFRLMSDQQIARDNRTACEWQSFGTDQAKLQNRFQFIFEAMGQLGTDPT 285
PHACH-LiPH8 PLP-------GEIRIQSDHTIARDSRTACEWQSFVNNQSKLVDDFQFIFLALTQLGQDPN 280
PLEOS-MnP4 PLP-------GEFRLQSDELLARDSRTSCEWQSFISNPNSMVPKFERAMAKMATLGQNPK 284
BJEAD-VP PLA-------GEIRLQSDADFARDSRTACEWQSFVNNQPRMQVLFKAAMQKLSILGHDLT 286
BB8-PLEER-VP PLQ-------GEIRLPSDHLLARDPQTACEWQSMVNNQPKIQNRFAATMSKMALLGQDKT 273
PLEOS-MnP5 PLR-------GEMRLQSDHLFARDDRTSCEWQSMTNDQQKIQDRFSDTLFKMSMLGQNQD 282
PLEOS-VP3 PLA-------GEIRLQSDHLLARDSRTSCEWQSMVDNMPKIQNRFAATMLKMSLLGQNQA 280
Consensus *: **:*: ** :: . .::* ** . : * . : :* :
AURDE-GP11 SLLDCSELIAQAPPATA--SQGFFPAGKTMEDLEIGCDAEAFPTTLVTQAGQPTMIPPVD 339
PHLRA-MnP2 DLVDCSAVVPVPKPATG--TPATFPASTGPQDLELTCTTEPFPTL-STAPGAQQTLIPHC 342
PHACH-MnP1 SLIDCSDVVPVPKPATG--QPAMFPASTGPQDLELSCPSERFPTL-TTQPGASQSLIAHC 341
BJEAD-LiP NMIDCSEVIPIPRNLTS-AQIPHFPAGKTIRDVEAACPETPFPRL-PTDAGRPTAVAPVP 344
PHLRA-LiP3 TLIDCSDVLPVPPPL---STVPHFPAGITINDVEPACAETPFPTL-PTDPGPATAVAAVP 341
PHACH-LiPH8 AMTDCSDVIPQSKPIPGNLPFSFFPAGKTIKDVEQACAETPFPTL-TTLPGPETSVQRIP 339
PLEOS-MnP4 KLIDCSEVIPVPRGR---VKQPTLPAGKTIKDIEASCRKAPFPRL-PTDKGTFTSILPVP 340
BJEAD-VP QMIDCSDVIPVPPST--AVRGSHLPAGNTLDDIEQACASTPFPTL-TADPGPATSVAPVP 343
BB8-PLEER-VP KLIDCSDVIPTPPAL---VGAAHLPAGFSLSDVEQACAATPFPAL-TADPGPVTSVPPVP 329
PLEOS-MnP5 AMIDCSDVIPVPAAL---VTKPHLPAGKVRTDVEQACATDAFPAL-AADPGPVTSVPRVP 338
PLEOS-VP3 DLIDCSDVIPTPPAL---VGKAHLPAGKVQSDVEQACATTPFPAI-AADPGPVTAVPPVP 336
Consensus : *** :: :**. *:* * ** : * :

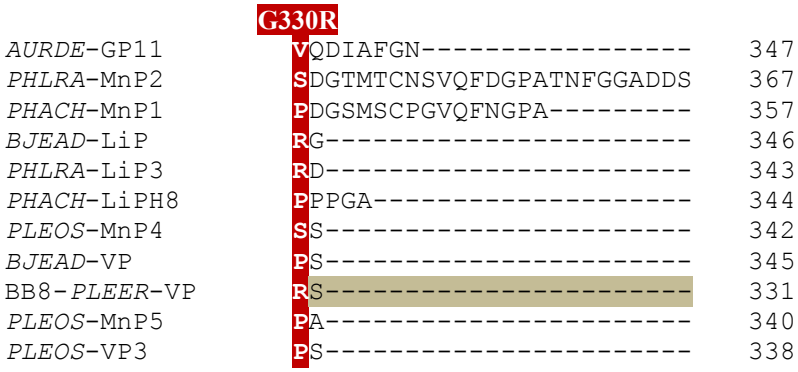

Fig. S2 MSA of representative ligninolytic peroxidases.

Sequences were obtained from the Uniprot database and aligned together with BB-8-*PLEER*-VP (the VP mutant from *Pleurotus eryngii*, O94753; obtained in the present study) using the Clustal Omega server (http://www.ebi.ac.uk/Tools/msa/clustalo/). The accession numbers used in the MSA were: *AURDE*-GP11 (GP11 from *Auricularia delicata;* J0WUI3); *PHLRA*-MnP2 (MnP2 from *Phlebia radiata;* Q70LM3); *PHACH*-MnP1 (MnP1 from *Phanerochaete chrysosporium;* Q02567); *BJEAD-LiP* (LiP from *Bjerkandera adusta;* W8YN06); *PHLRA*-LiP3 (LiP3 from *Phlebia radiata;* Q53WT9); *PHACH*-LiPH8 (LiPH8 from *Phanerochaete chrysosporium;* P06181); *PLEOS*-MnP4 (MnP4 from *Pleurotus ostreatus;* A0A067NYV2); *BJEAD*-VP (VP from *Bjerkandera adusta;* W8YE46); *PLEPU*-MnP5 (MnP5 from *Pleurotus pulmonarius;* Q2VT17); *PLEOS*-VP3 (VP3 from *Pleurotus ostreatus;* A0A067NKY1). The mutations in the stabilizing backbone are highlighted in red, those mutations that promote functional expression in yeast in cyan, and the mutations driving activity at alkaline pHs in dark brown, orange and green.

	AURDE-GP11	*PHLRA*-MnP2	*PHACH*-MnP1	*BJEAD*-LiP	*PHLRA*-LiP3	*PHACH*-LiPH8	*PLEOS*-MnP4	*BJEAD*-VP	BB8-*PLEER*-VP	*PLEOS*-MnP5	*PLEOS*-VP3
AURDE-GP11	**100**	45.9	46.3	43.5	43.3	45.2	46.0	48.5	47.0	43.0	44.6
PHLRA MnP2	45.9	**100**	72.8	41.7	45.0	47.6	48.0	52.7	48.6	49.5	49.4
PHACH-MnP1	46.3	72.8	**100**	43.6	47.4	47.3	50.6	56.8	52.9	50.6	51.0
BJEAD-LiP	43.5	41.7	43.6	**100**	61.1	58.5	54.4	59.9	56.8	57.0	56.0
PHLRA-LiP3	43.3	45.0	47.4	61.1	**100**	63.2	50.4	58.8	54.2	52.2	53.3
PHACH-LiPH8	45.2	47.6	47.3	58.5	63.2	**100**	55.2	64.3	55.9	54.2	56.5
PLEOS-MnP4	46.0	48.0	50.6	54.4	50.4	55.2	**100**	62.6	63.1	53.7	59.5
BJEAD-VP	48.5	52.7	56.8	59.9	58.8	64.3	62.6	**100**	69.5	62.0	67.3
BB8-*PLEER*-VP	47.0	48.6	52.9	56.8	54.2	55.9	63.1	69.5	**100**	66.8	75.5
PLEOS-MnP5	43.0	49.5	50.6	57.0	52.2	54.2	53.7	62.0	66.8	**100**	81.0
PLEOS-VP3	44.6	49.4	51.0	56.0	53.3	56.5	59.5	67.3	75.5	81.0	**100**

Identity Matrix from MSA

SUPPLEMENTAL EXPERIMENTAL PROCEDURES

Reagents and strains

ABTS (2,2'-azino-bis(3-ethylbenzothiazoline-6-sulfonic acid)), 2,6-DMP (2,6-Dimethoxyphenol), Reactive black 5 (RB5), sinapic acid, guaiacol, veratryl alcohol, syringaldazine, catechol, Manganese sulphate, *Taq* DNA polymerase, bovine hemoglobin, hemin from bovine, Horseradish peroxidase (HRP) and the *S. cerevisiae* transformation kit were purchased from Sigma-Aldrich (Madrid, Spain). Hydrogen peroxide 30 % (v/v) was obtained from Merck Millipore (Darmstadt, Germany). *Pfu*-Ultra polymerase, *Escherichia coli* XL1-Blue chemocompetent cells and the GeneMorph II Kit (mutazyme II polymerase) were from Stratagene (La Jolla, CA, USA). The Zymoprep Yeast Plasmid Miniprep Kit was obtained from Zymo-Research (Orange, CA, USA). The Low melting point agarose was from Bio-Rad (Hercules, CA), the NucleoSpin and PCR clean-up kit from Macherey-Nagel (Düren, Germany) and the *Bam*HI and *Xho*I restriction enzymes from New England Biolabs (Hertfordshire, U.K.). The protease-deficient *S. cerevisiae* strain BJ5465 (α ura3-52 trp1 leu2Δ1 his3Δ200 pep4::HIS3 prb1Δ1.6R can1 GAL) was from LGCPromochem (Barcelona, Spain). The oligonucleotides used along the evolutionary process were purchased from Isogen Life Science (De Meern, The Netherlands). All chemicals were of reagent-grade purity.

Culture media

Synthetic complete (SC, minimum medium) contained 0.67% (w/v) yeast nitrogen base, 1.92 g/L yeast synthetic drop-out medium supplement without uracil, 2% (w/v) D-raffinose and 25 μg/mL chloramphenicol. SC-Hemin medium contained the recipe for SC plus bovine hemin (25 g/L) and 67 mM KH_2PO_4 buffer (pH 6.0). YP (1.55x) medium contained 10 g yeast extract, 20 g peptone and ddH_2O to 650 mL. Microplate expression medium (YP-Hb)

contained 720 mL YP (1.55x), 67 mL 1 M KH_2PO_4 buffer (pH 6.0), 111 mL 20% (w/v) D-galactose, 100 mg/L bovine hemoglobin, 1 ml 25 g/L chloramphenicol and ddH_2O to 1000 mL. Microplate YP-EtOH expression medium contained 720 mL YP (1.55x), 67 mL 1 M KH_2PO_4 buffer (pH 6.0), 111 mL 20% (w/v) D-galactose, 25 g/L ethanol absolute, 1 ml 25 g/L chloramphenicol and ddH_2O to 1000 mL. YPD solution contained 1% (w/v) yeast extract, 2% (w/v) peptone, 2% (w/v) D-glucose and 25 µg/mL chloramphenicol. Flask expression medium contained 720 mL YP (1.55x), 67 mL 1 M KH_2PO_4 buffer (pH 6.0), 111 mL 20% (w/v) D-galactose, 25 g/L ethanol absolute, 500 mg/L bovine hemoglobin, 1 mM $CaCl_2$, 1 mL 25 g/L chloramphenicol and ddH_2O to 1,000 mL. SC drop-out plates contained 0.67% (w/v) yeast nitrogen base, 1.92 g/L (w/v) yeast synthetic drop-out medium supplement without uracil, 2% (w/v) bacto agar, 2% (w/v) D-glucose and 25 µg/mL chloramphenicol. Luria-Bertani (LB) medium was prepared with 1% (w/v) peptone, 0.5% (w/v) yeast extract, 1% (w/v) NaCl and 100 µg/mL ampicillin and in the case of drop-out plates LB/amp plus 2% (w/v) bacto agar.

Re-screenings

First re-screening: Aliquots of 5 µL of the best clones were removed from the master plates and used to inoculate 50 µL of SC minimal medium (SC-Hemin 1st generation) in new 96-well plates. Columns 1 and 12, and rows A and H, were not used to prevent the appearance of false positives. After incubating for 24 h at 30 °C, 225 rpm, and 80% relative humidity, 5 µL was transferred to the adjacent wells and incubated for a further 24 h. Finally, 160 µL of YP-Hb microplate expression medium (YP-EtOH for 1st generation) was added and the plates were incubated for another 24 h. Accordingly, each mutant was grown in 4 wells. The parental types were subjected to the same procedure (row D, wells 7-11) and the plates were assessed using the same protocols as those used for the HTS-screening protocol.

Second re-screening: An aliquot from the wells with the best clones in the first re-screening was inoculated in 3 mL of YPD and incubated at 30 °C and 225 rpm for 24 h, recovering the plasmids from these cultures (Zymoprep Yeast Plasmid Miniprep Kit). As the product of the zymoprep was very impure and the concentration of DNA extracted very low, the zymoprep mixtures containing shuttle vectors were transformed into super-competent *E. coli* cells (XL1-Blue, Stratagene) and plated on LB/amp plates. Single colonies were picked and used to inoculate 5 mL LB/amp media, and they were grown overnight at 37 °C and 225 rpm. The plasmids were then extracted (NucleoSpin Plasmid kit, Macherey-Nagel, Germany) and *S. cerevisiae* suspension was transformed with plasmids from the best mutants as well as with the parental type. Five colonies for each mutant were selected and re-screened as described above.

Third re-screening (determination of pH profiles, kinetic thermo-stabilities and pH stabilities): A single colony from the *S. cerevisiae* clone containing the parental 2-1B, the new mutants and untransformed yeast were picked from a SC drop-out plate (SC supplemented with uracil for untransformed cells), inoculated into 5 mL of minimal medium and incubated for 48 h at 30 °C and 225 rpm (Orbitron-INFORS, Biogen, Spain). An aliquot of cells was removed and used to inoculate a final volume of 5 mL of minimal medium in a 50 mL falcon tube (optical density, OD_{600} = 0.3), and they were incubated until two growth phases were completed (6-8 h, OD_{600} = 1). Thereafter, 9 mL of flask expression medium (500 mg/L bovine hemoglobin) was inoculated with 1 mL of this pre-culture in a 100 mL flask (OD_{600} = 0.1). After incubating for ~48 h at 30 °C and 225 rpm (maximal VP activity; OD_{600} = 25-30), the cells were separated by centrifugation for 15 min at 3,000 rpm and 4 °C (Eppendorf 5810R Centrifuge with F-34-6-38 rotor, Germany), and the supernatants were collected and stored at 4 °C.

pH activity profile: Parental type (2-1B) and the mutant winners of each round of evolution were assayed for activity in a pH range from 2 to 9. Aliquots (20 µL) of crude supernatants from *S. cerevisiae* were diluted to give a linear response in kinetic mode. Then, 180 µL of reaction mixture were added using a Multidrop station (Multidrop Combi, ThermoFischer Scientific,Vantaa, Finland). The final concentrations of reaction mixture per well were 100 mM citrate-phosphate-borate buffer at different pH (2-10), 0.1 mM of H_2O_2 and 2 mM ABTS. The absorbance was recorded at 418 nm in kinetic mode using the plate reader.

pH stability assay: Appropriate dilutions of the supernatants were prepared such that aliquots (20 µL) produced a linear response in kinetic mode. Each variant was diluted in 100 mM citrate-phosphate-borate buffer with pH ranging from 3.0-10.0. Aliquots of 20 µL were removed during 144h and measured in the presence of 180 µL of reaction. The final concentrations in the well were 100 mM citrate-phosphate-borate buffer pH 4.0, 0.1 mM of H_2O_2 and 2 mM ABTS. The absorbance was monitored at 418 nm in kinetic mode using a plate reader.

Thermostability assay (T_{50}): A gradient profile was constructed using a thermocycler (Mycycler, Bio-Rad, USA) for the selected mutants and the parental type, using 50 µL for each point in a gradient scale ranging from 30 to 80 °C. After a 10 min incubation, samples were removed and chilled on ice for 10 min. Thereafter, 20 µL samples were removed and incubated for 5 min at room temperature. Finally, 180 µL of 100 mM sodium tartrate buffer (pH 4.0), 2 mM ABTS and 0.1 mM H_2O_2 was added to the samples to measure activities. The thermostability values were calculated as the ratio between the residual activity at different temperature points and the initial activity at room temperature.

Production and Purification of VP variants

A single colony from transformed yeast cells was used to inoculate 20 mL of SC minimal medium (in a 100 mL flask) and incubated for 48h at 30 °C and 220 rpm (Orbitron-INFORS, Biogen, Spain). Then, OD_{600} was measured and this pre-culture used to inoculate 120 mL of minimal medium in a 250 ml flask (OD_{600}= 0.3). They were incubated until two growth phases had been completed (6-8 h, OD_{600} = 1) and thereafter, 450 mL of flask expression medium (500 mg/L bovine hemoglobin) was inoculated with 50 mL of this pre-culture in a 2 litre baffled flask (OD_{600}= 0.1). The cultures were incubated for 48h at 30 °C and 230 rpm (Micromagmix shaker) and the maximal VP activity reached (OD_{600} =25–30); the cells were recovered by centrifugation at 5,000 rpm for 30 min at 4 °C (Avanti J-E centrifuge Beckman Coulter with JA-14 rotor, Fullerton, CA). The supernatant was collected and triple filtered (through filter paper, a glass fibre filter and then a nitrocellulose membrane of 0.45 µm pore size).

Purification protocol: VP crude extracts were first submitted to a fractional precipitation with ammonium sulphate (50-75%). Samples were pelleted at 12,000 rpm, 15 min and 4 °C (Avanti J-E centrifuge Beckman Coulter with JA-14 rotor). The final pellet was recovered and dialyzed in 20 mM piperazine buffer (buffer P, pH 5.5), then the sample was filtered and loaded on to the FPLC (Äkta Purifier; GE Healthcare Uppsala, Sweden) coupled with a strong anion-exchange column (HiTraP QFF; GE Healthcare Uppsala, Sweden) pre-equilibrated with buffer P. The proteins were eluted with a linear gradient from 0 to 1 M of NaCl in two phases at a flow rate of 1 ml/min: from 0 to 25% over 60 min and from 25 to 100% over 5 min. Fractions with VP activity were pooled, concentrated and dialysed against buffer P with a stirred ultrafiltration cell and an ultracell 10 kDa ultrafiltration Disc of 44.5 mm (Amincon cell, Merck

Millipore, Germany). Thereafter, samples were loaded onto a HPLC–PDA column coupled with a 10 µm high resolution anion-exchange Biosuite Q (Waters) pre-equilibrated with buffer P. The proteins were eluted on a linear gradient from 0 to 1 M NaCl at a flow rate of 1 ml/min in two phases: from 0 to 6% in 30 min, and from 6 to 100% in 5 min. The fractions with VP activity were pooled, dialysed against 10 mM sodium tartrate buffer (pH 5.0), concentrated and stored at 4 °C. Throughout the purification protocol, the fractions were analysed by SDS/PAGE on 12% gels and the proteins were stained with colloidal Coomassie Blue (Protoblue Safe, National Diagnostics). Purified VP concentrations were determined spectrophotometrically (SHIMADZU UV-1800 spectrophometer, Columbia, MD, USA) in 1 mL quartz cuvettes with molar extinction coefficient for VP at 407nm (ε_{VP} =150,000 M^{-1}. cm^{-1}).The Reinheitszahl values (R_z: Abs_{407}/Abs_{280}) obtained were above 2.